Comparative Analysis of a novel Cascade Transcritical Carbon Dioxide cycle and Split Transcritical Carbon Dioxide cycle integrated with Advanced Absorption Refrigeration system.

Submitted By

Tahamid Arshil

190012145

Estiak Ahmed

190011114

Supervised By

Dr. Mohammad Monjurul Ehsan

A Thesis submitted in partial fulfillment of the requirement for the degree of Bachelor of Science in Mechanical Engineering

Department of Mechanical and Production Engineering (MPE)

Islamic University of Technology (IUT)

July, 2024

Candidate's Declaration

This is to certify that the work presented in this thesis, titled, "Comparative Analysis of a novel Cascade Transcritical Carbon Dioxide cycle and Split Transcritical Carbon Dioxide cycle integrated with Advanced Absorption Refrigeration system.", is the outcome of the investigation and research carried out by me under the supervision of Dr. Mohammad Monjurul Ehsan, Professor, Department of Mechanical and Production Engineering, Islamic University of Technology.

It is also declared that neither this thesis nor any part of it has been submitted elsewhere for the award of any degree or diploma.

Tahamid Arshil
Student No: 190012145

Estiak Ahmed
Student No: 190011114

Recommendation of the Thesis Supervisors

The thesis titled "Comparative Analysis of a novel Cascade Transcritical Carbon Dioxide cycle and Split Transcritical Carbon Dioxide cycle integrated with Advanced Absorption Refrigeration system." submitted by Tahamid Arshil, Student No: 190012145 and Estiak Ahmed, Student No: 190011114 has been accepted as satisfactory in partial fulfillment of the requirements for the degree of B Sc. in Mechanical Engineering **on 28th June, 2024.**

1. ----------
   Dr. Mohammad Monjurul Ehsan (Supervisor)
   Professor
   MPE Dept., IUT, Board Bazar, Gazipur-1704, Bangladesh.

CO-PO Mapping of IPE 4800 -Theis and Project

COs	Course Outcomes (CO) Statement	(PO)	Addressed by	
CO1	Discover and Locate research problems and illustrate them via figures/tables or projections/ideas through field visit and literature review and determine/Setting aim and objectives of the project/work/research in specific, measurable, achievable, realistic and timeframe manner.	**PO2**	Thesis Book	
			Performance by research	
			Presentation and soft skill	
CO2	Design research solutions of the problems towards achieving the objectives and its application. Design systems, components or processes that meets related needs in the field of mechanical engineering	**PO3**	Thesis Book	
			Performance by research	
			Presentation and soft skill	
CO3	Review, debate, compare and contrast the relevant literature contents. Relevance of this research/study. Methods, tools, and techniques used by past researchers and justification of use of them in this work.	**PO4**	Thesis Book	
			Performance by research	
			Presentation and soft skill	
CO4	Analyse data and exhibit results using tables, diagrams, graphs with their interpretation. Investigate the designed solutions to solve the problems through case study/survey study/experimentation/simulation using modern tools and techniques.	**PO5**	Thesis Book	
			Performance by research	
			Presentation and soft skill	
CO5	Apply outcome of the study to assess societal, health, safety, legal and cultural issue and consequent possibilities relevant to mechanical engineering practice.	**PO6**	Thesis Book	
			Performance by research	
			Presentation and soft skill	
CO6	Relate the solution/s to objectives of the research/work for improving desired performances including economic, social and environmental benefits.	**PO7**	Thesis Book	
			Performance by research	
			Presentation and soft skill	
CO7	Apply moral values and research/professional ethics throughout the work, and justify to genuine referencing on sources, and demonstration of own contribution.	**PO8**	Thesis Book	
			Performance by research	
			Presentation and soft skill	
CO8	Perform own self and manage group activities from the beginning to the end of the research/work as a quality work.	**PO9**	Thesis Book	
			Performance by research	
			Presentation and soft skill	
CO9	Compile and arrange the work outputs, write the report/thesis, a sample journal paper, and present the work to wider audience using modern communication tools and techniques.	**PO10**	Thesis Book	
			Performance by research	
			Presentation and soft skill	
CO10	Organize and control cost and time of the work/project/research and coordinate them until the end of it.	**PO11**	Thesis Book	
			Performance by research	
			Presentation and soft skill	
CO11	Recognize the necessity of life-long learning in career development in dynamic real-world situations from the experience of completing this project.	**PO12**	Thesis Book	
			Performance by research	
			Presentation and soft skill	

Student Name /ID:

1……..

2. ……..

3. ……..

Signature of the Supervisor: ……

Name of the Supervisor: ……..

K-P-A Mapping of IPE 4800 -Theis and Project

COs	POs	Related Ks								Related Ps							Related As				
		K1	K2	K3	K4	K5	K6	K7	K8	P1	P2	P3	P4	P5	P6	P7	A1	A2	A3	A4	A5
CO1	PO2																				
CO2	PO3																				
CO3	PO4																				
CO4	PO5																				
CO5	PO6																				
CO6	PO6																				
CO7	PO8																				
CO8	PO9																				
CO9	PO10																				
CO10	PO11																				
CO11	PO12																				

Student Name /ID:

1……..

2. ……..

3. ……..

Signature of the Supervisor: ……

Name of the Supervisor: ……..

Acknowledgment

In the Name of Allah, the Most Beneficent, the Most Merciful First of all, I am grateful to ALLAH (SWT), the most benevolent and kind to provide me the strength and ability to write this dissertation. I want to thank my project supervisor, Dr. Mohammad Monjurul Ehsan, for his strong and patient support through unpredictable problems during the project and his precious advice when I faced difficulties. His generosity, kindness and strong supervision during work made me feel less stressed in confronting unexpected troubles and be more productive in my personal life.

In the next step, I would like express my deep acknowledgment to my father and mother for their continued support and dedication towards my higher study.

Abstract

A transcritical carbon dioxide (t-CO_2) Rankine cycle is capable of achieving high efficiency for waste heat recovery (WHR) from a gas turbine, despite being simpler and more compact than a steam/water cycle. Regarding the Waste Heat Recovery (WHR) system, it is crucial to optimize the net output power by integrating the necessary components. The waste heat utilization efficiency is combined with the thermal efficiency of the cycle. A basic T-CO_2 Rankine cycle employed for a high-temperature source is unable to completely harness the waste heat due to the fact that the working fluid is prepared to a high temperature by the recuperator in order to obtain a superior cycle efficiency. In order to utilize the unused waste heat in a simple cycle, one option is to incorporate a cascade cycle with a low-temperature (LT) loop alongside the high-temperature (HT) loop. Another option is to implement a split cycle, where the flow after the pump is divided and preheated separately by the recuperator and LT heater before being used by the HT heater. This study provides a comparative analysis of three cycles, focusing on the energy and exergy studies of their respective systems. The findings indicate that a split cycle has the capacity to generate the most amount of power among the three systems examined, across a broad spectrum of operating conditions. The rationales for this are elucidated extensively. This research aims to address this significant problem by optimizing waste heat recovery (WHR) strategies. By effectively capturing and utilizing waste heat, we can reduce overall energy consumption and reliance on fossil fuels. Also, we can Increase the efficiency of industrial processes and power generation as well as mitigate greenhouse gas emissions and contribute to climate change mitigation. However, technical limitations of modeling and matching appropriate WHR technologies to diverse waste heat sources with varying temperatures and flow rates can be a significant challenge for the proposed solutions. This study looks at various configurations of Supercritical Carbon dioxide Rankine cycles and compares their performance which leads to positive findings in favor of the split configuration. The other configurations investigated were simple and cascade cycles. These advanced configurations of Rankine cycles can yield never-before-achieved performance for power cycles. However, regardless of their efficiency, there is always some waste heat that is discharged into the environment. This study aims to capture the waste heat through a novel system. The novel system involves the Rankine cycle integrated as the top cycle acting as the source of waste heat with an advanced absorption refrigeration system as the bottom cycle. The fitness and constraints of the overall system is investigated and compared with prior findings and an attempt to justify the performance is the domain of this work. The following work owing to being a preliminary study for the final work, the study for now validates developed models against the reference models obtained from literature review. Such validation facilitates the undertaking of the integration task. The fitness and constraint modelling of the novel integrated system yield unexpected result owing to erratic governing equations of the performance parameters. However, validated state point calculations are enough to lay the groundwork for the tuning of the performance evaluation of the novel system. This paper tries to present a comparative study of two different configurations of the novel system, each cycle integrating four cycles in total. Hence, the complexity of such modelling depends on a number of parameters. And such models can project different behavior when evaluated under a broad range of working parameters of different components involved in the system. These parameters can be tweaked to facilitate multivariable optimization of desired performance parameters and fitness constraints. Such work further needs the support of strong optimization algorithm paired with machine learning. Hence, the domain of the present work can be further broadened to determine the optimal working conditions of the novel systems.

Keyword: Cascade Transcritical; Split Transcritical; Second law efficiency; Exergy analysis; Absorption cycle; Comparative analysis.

Table of Contents

List of Figures

List of Tables

Nomenclatures and Symbol

Table 1: Nomenclature

HFC	Hydrofluorocarbon
FT	Flash tank
Ti	Temperature [◦C]
Pi	Pressure [kPa]
Hi	Enthalpy [kJ kg− 1]
Si	Entropy [kJ kg− 1 K− 1]
$\dot{w}_{comp}$	Compressor load [kW]
$\dot{E}_D$	Rate of Exergy destruction [kW]
$\dot{Q}$	Heat transfer rate [kW]
η_{II}	Exergetic efficiency [dimensionless]
η_{is}	Isentropic efficiency [dimensionless]
E	Effectiveness of heat exchanger
i	Stream (1, 2, 3 … … ….)
0	Dead state point
evp	Evaporator
cond	Condenser
abs	Absorber
gen	Generator
comp	Compressor
Cp	isobaric specific heat [kJ/(kgK)]
E	exergy (kJ)
$\dot{E}$	rate of exergy (kW)
ε	heat exchanger effectiveness
h	specific enthalpy (kJ/kg)
HT	high temperature
k	specific exergy (kJ/kg)
L	exergy loss (kJ)
$\dot{L}$	rate of exergy loss (kW)
LT	low temperature
m	mass (kg)
$\dot{m}$	mass flow rate (kg/s)
P	pressure (kPa)
Q	heat (kJ)
s	specific entropy [kJ/(kgK)]
S-CO_2	supercritical CO_2
T	temperature (K)
W	work (kJClick or tap here to enter text.)
X	split ratio
η	isentropic efficiency
Subscripts	
0	atmospheric (environmental) state
C	condenser
cyc	cycle
e	expander
EG	exhaust gas

P	pump
CO_2	carbon dioxide
H	heater
HR	heat recovery
i	state point
in	inlet
max	maximum
net	net output
out	outlet
P	pump
R	recuperator
s	isentropic
Sys	System
Superscripts	
T	turbine
+	input
-	Output

Chapter 1: Introduction

1.1 Introduction

The increased need for energy and growing concerns about environmental sustainability necessitate the development of efficient and ecologically friendly energy systems. Traditional power-generating methods frequently struggle with poor efficiency and significant heat rejection, resulting in energy loss and higher greenhouse gas emissions. Furthermore, contemporary structures and industrial operations demand both cooling and electricity generation. Conventional systems handle these demands individually, which increases energy losses and environmental consequences. This study addresses the requirement for a high-efficiency, environmentally friendly integrated power and cooling system. Current methods frequently have downsides, such as Low overall efficiency: Conventional power-producing methods generate a lot of waste heat, and separate cooling systems need more energy. Traditional power generation methods rely on fossil fuels, contributing to greenhouse gas emissions.

Furthermore, the refrigerants used in some cooling systems may be environmentally harmful. Most systems are built to meet specified power or cooling requirements, restricting their capacity to adjust to changing conditions. This research suggests combining a transcritical carbon dioxide (CO_2) Rankine cycle as the top cycle with an absorption refrigeration system for the bottom cycle. This hybrid system has various potential benefits. The transcritical CO_2 cycle runs at greater pressures and temperatures than typical Rankine cycles, resulting in increased thermodynamic efficiency. Waste heat from the top cycle can be used by the bottom cycle to provide cooling, reducing overall energy loss. CO_2 is a naturally occurring, non-toxic refrigerant that has a minimal global warming potential.

Furthermore, the system's capacity to efficiently use waste heat decreases reliance on fossil fuels and their related emissions. Flexibility: The system may be configured to fulfill a variety of power and cooling requirements by altering the operating parameters of both cycles. This study is based on breakthroughs in numerous fundamental technologies. Transcritical CO_2 Rankine Cycle: This technique uses CO_2's unique thermodynamic features to produce high efficiency and compact system design. System integration and optimization: Advanced modeling and control techniques are used to improve the integrated system's performance under varied operating situations. Overall, the study aims to demonstrate the justification & possible advantages added owing to combining the transcritical CO_2 Rankine cycle with an absorption refrigeration system for power and cooling[2]. By using these modern technologies, we may help to construct sustainable and efficient energy systems for the future.

1.2 Research scope and problem statement formulation

The purpose of this study is to examine how waste heat recovery can be achieved by combining an absorption refrigeration system with a transcritical carbon dioxide (CO_2) Rankine cycle. Creating a thorough design for the integrated thermodynamic system, determining the parts and setups required for a smooth integration, and guaranteeing the best possible thermal and fluid dynamic compatibility are all included in the scope. To comprehend the interactions and performance traits of the integrated system, a thorough thermodynamic study will be carried out, identifying critical variables affecting efficiency such as temperature, pressure, and flow rates. To improve overall efficiency and dynamically modify operational parameters in response to fluctuating waste heat availability and demand,

optimization algorithms and control strategies will be created. The system's performance will be assessed using simulations and experimental research under various operating situations. Performance metrics will be compared with those of standalone systems and traditional waste heat recovery techniques. A cost-benefit analysis will be used in the research to evaluate the integrated system's economic viability and determine its capital, operating, and payback periods. Environmental impact assessments will examine the lifecycle environmental impact for long-term ecological advantages, with a focus on greenhouse gas emission reductions and general sustainability. The integrated system will be compared to current waste heat recovery technologies in order to determine which industrial sectors it delivers the greatest gains in energy efficiency and waste heat use. The inefficiency of traditional waste heat recovery systems in industrial settings, which results in significant energy losses and environmental effect, is the main issue this research attempts to address. Although absorption refrigeration systems and transcritical CO_2 Rankine cycles independently present viable options, their combined potential is still underutilized. This study aims to create, assess, and optimize an integrated system that provides efficient refrigeration and maximizes energy recovery from waste heat, advancing waste heat recovery technologies and providing an eco-friendly and more productive industrial energy management solution.

In this comparative analysis, the two systems—cascade and split—that make up the two distinct Rankine cycle layouts are used. The system's total efficiency is increased when two transcritical CO_2 (tCO_2) cycles are cascaded using a heater in the cascade configuration. This allows the first cycle's waste heat to be used in the second cycle. The split arrangement, on the other hand, splits the stream before it reaches the heater, allowing for the simultaneous distribution and use of heat across various cycle parts. The waste heat produced by these cycles serves as the top power cycle in the system integration, and the absorption refrigeration system (ARS) uses the waste heat from these cycles. The purpose of the study is to evaluate and contrast the two layouts' functionality, economy, and suitability in terms of energy recovery, running expenses, and environmental effect. The goal of the research is to identify the best system design for optimizing waste heat use and raising the general effectiveness of industrial waste heat recovery systems by analyzing these two configurations.

Chapter 2: Literature Review

2.1 Characteristics of Transcritical CO_2 power cycles

The S-CO_2 Rankine cycle is a power cycle in which supercritical carbon dioxide is used as the working fluid. It is intended to operate at high temperatures and pressures, making it suitable for high-temperature heat sources used in concentrated solar power, nuclear, and fossil fuel power plants. In this cycle, a recuperator recovers heat from the exhaust stream and warms the carbon dioxide working fluid before it reaches the main turbine[8]. The recuperator is a crucial component for increasing the cycle's thermal efficiency by transferring heat from the high-temperature exhaust to the incoming fluid, hence lowering the amount of heat required in the combustion or heat source. However, the efficiency of a single-recuperated S-CO_2 Rankine cycle is limited. To maintain the cycle's overall high thermal efficiency, the recuperator increases the temperature of the working fluid[9]. As a result, the working fluid exiting the recuperator is already relatively hot, and there is little room for additional heat addition without surpassing the critical temperature of carbon dioxide. To circumvent this limitation and make use of the residual waste heat, numerous cycle configurations with additional components have been proposed. A secondary loop or reheat cycle is one typical strategy. In a reheat cycle, the working fluid is partially inflated and then reheated before entering a second turbine following the first cycle's main turbine[10]. This enables more heat addition and expansion, giving the chance to use more of the available waste heat. The major purpose is to capture as much energy as possible from the high-temperature heat source by cleverly structuring the cycle arrangement. Engineers intend to increase the overall efficiency and performance of the S-CO_2 Rankine cycle by including reheat or other advanced cycle designs, allowing it to recover waste heat more effectively from high-temperature sources. Cho et al. compared the performance of several Supercritical Carbon Dioxide (S-CO_2) cycle configurations as bottoming power systems to that of a steam Rankine cycle in the context of a natural gas combined-cycle power plant. The goal was most likely to evaluate the viability of S-CO_2 cycles as an alternative to traditional steam Rankine cycles in the context of combined-cycle power generation, with a focus on increasing overall plant efficiency. Huck emphasized the competitiveness of S-CO_2 cycles, especially about specific steam-bottoming cycle designs[11]. The decision between S-CO_2 and steam cycles is determined by the gas turbine's characteristics and the application's specific requirements. Furthermore, the integration of thermoelectric generating systems with S-CO_2 cycles has been proposed to improve power recovery in specific circumstances, such as marine applications[12]. Engineers performed a thermoeconomic analysis on five supercritical-CO_2 waste heat recovery (WHR) systems for a twenty-five MWe gas turbine[1]. The S-CO_2 cycles studied included a single-recuperated Brayton cycle, a cascade cycle, a dual-recuperated cycle, and a split cycle (also known as a preheating cycle). The split-cycle provided the maximum net electric power from the waste heat source of the four cycles evaluated. Two S-CO_2 cycles were combined to recover the residual heat from the cascade and dual-recuperated cycles. The cascade cycle divides the compressor outlet flow into high temperature (HT) and low temperature (LT). The HT stream bypassed the recuperator and went directly through a main heater to recover gas turbine waste heat, whereas the LT stream went via an LT recuperator followed by an HT recuperator to collect the residual heat from the enlarged HT stream[13]. In the split cycle, the flow following the compressor was split, with one stream prepared by the recuperator and the other by the LT heater separately. The two streams were then merged and sent through the same HT heater and turbine. Wright et al. showed that the split cycle produced the maximum net electric power from waste heat when compared to the other cycles.

Another paper studied the feasibility of adopting an indirect supercritical CO_2 (SCO_2) cycle replacing the typical 'He' cooled cycle for gas-cooled fast reactors (GFRs)[14]. They compare the performance and practicality of various indirect power cycle alternatives. Helium-nitrogen: In the main loop of the Brayton cycle, the working fluid is a combination of helium and nitrogen, and heat is transferred to a secondary SCO_2 loop via an intermediate heat exchanger[5]. The supercritical water Rankine cycle employs water in the main loop, similar to standard light-water reactors, but operates at supercritical pressures for better efficiency. SCO_2 Recompression Brayton Cycle: This cycle uses pure SCO_2 in both the primary and secondary loops, with three variations studied. Basic Design: SCO_2 turbine inlet temperature is 550°C. SCO_2 turbine inlet temperature is 650°C[6]. Maintains the turbine intake temperature at 650°C while reducing the compressor inlet temperature to improve efficiency. The indirect SCO_2 recompression cycle emerges as the most appealing alternative. Separating the helium and CO_2 loops simplifies maintenance and eliminates radioactive contamination hazards. Operating at lower temperatures simplifies primary system design and enhances safety. It Achieves efficiencies comparable to the reference GFR direct cycle design, and even slightly higher in some advanced setups[5]. SCO_2 cycle components are more compact, potentially resulting in cheaper capital expenditures. A smaller GFR core due to lower operating temperatures allows for a smaller and less expensive containment structure. Hejzlar et al.'s work builds upon previous research on GFRs and SCO_2 cycles[15]. Their study confirms the potential benefits of SCO_2 cycles for better efficiency and reduced thermal stresses in GFRs, as suggested by previous studies (e.g., Dostal et al., $_2$004). It provides a full analysis of several indirect cycle choices and their advantages and limitations, providing significant insights for future GFR design decisions. It also Introduces the notion of employing recompression in the SCO_2 cycle to improve efficiency and meet the challenges of high-pressure operation. However, the research focuses on theoretical analysis and modeling, which necessitates additional experimental validation and techno-economic assessments. Further research into material compatibility and long-term performance of components under SCO_2 settings is required[1]. A detailed examination of the transient and safety behavior of the indirect cycle in comparison to the direct cycle is required.

Other studies looked into the benefits and cons of using transcritical (T-CO_2) and supercritical (S-CO_2) CO_2 cycles in power generation systems with access to both low- and high-temperature heat sources. They are focused with pushing the boundaries of traditional cycle designs for such applications[16]. Key discoveries include T-CO_2 Rankine cycles are more effective for harnessing low-temperature heat. The T-CO_2 Rankine cycle, with its high specific heat and reduced compression effort, is ideally suited for heat recovery at lower temperatures than T-CO_2 Brayton cycles or recompression S-CO_2 cycles. Partial condensation T-CO_2 or recompression S-CO_2 cycles are useful for high-temperature heat usage. By partly condensing the working fluid prior to high-temperature heat input, these cycles diminish internal irreversibility in the recuperator, resulting in better efficiency for high-temperature sources[17]. Hybrid cycle arrangements provide the following benefits: Integrating T-CO_2 Rankine and T-CO_2 Brayton cycles, as well as recompression S-CO_2 cycles, may effectively use both low- and high-temperature heat sources while maintaining high overall efficiency. There are trade-offs between cycle complexity and efficiency: While hybrid cycles are more efficient, they require more components and controls, which increases system complexity and possible maintenance costs. Kim et al.'s study expands on prior studies on T-CO_2 and S-CO_2 cycles for waste heat recovery and power production from a variety of sources[18]. They explain the notion of applying these cycles to systems with a variety of heat sources, offering insights into maximizing energy consumption in industrial processes and cogeneration systems. The research goes beyond the restrictions of classic T-CO_2 and S-CO_2 cycle configurations for specific heat source characteristics, offering alternative and hybrid cycle designs for increased efficiency[19]. The work focuses mostly on theoretical analysis and modeling, necessitating further experimental validation and

techno-economic assessments for practical application. Additional research is needed to optimize hybrid cycle topologies and component design for specific applications. The effect of transient operations and control techniques on system performance and stability necessitates further investigation. Overall, Kim et al.'s research makes an important addition to the field of T-CO_2 and S-CO_2 cycle applications by addressing the effective use of a variety of heating sources[20]. Their findings point to interesting future directions for study and development of enhanced power production systems with increased efficiency and flexibility. Investigation into supercritical CO_2[1] (sCO_2) cycles for waste heat to power (WH_2P) applications: The research looks at the possibility of sCO_2 cycles for converting low- and medium-grade waste heat (50-500°C) into power, which addresses a major difficulty in industrial energy efficiency. Kacludis et al. compare the sCO_2 cycle to proven WH_2P solutions such as organic Rankine cycles (ORC) and steam cycles, showing the benefits of sCO_2. Higher efficiency: sCO_2 cycles outperform ORC and steam cycles in comparable temperature ranges, resulting in more power generation from the same waste heat source. Due to the increased density of CO_2, sCO_2 systems require smaller equipment, potentially saving space and money for WH_2P installations. S-CO_2 cycles can adapt to different heat source profiles and work effectively with a variety of waste heat streams. The study demonstrates the possible uses of sCO_2 WH_2P technology in many sectors, including Combined cycle gas turbines use waste heat from gas turbines in power plants to generate extra electricity. Waste heat from engines is recovered and utilized in power generation or industrial activities[21]. Energy-intensive manufacturing involves recovering waste heat from a variety of industrial operations such as steel and metal production, cement making, and so on. Kacludis et al.'s research demonstrates the promising potential of sCO_2 WH_2P technology for increasing industrial energy efficiency and lowering greenhouse gas emissions. Their findings led to the increased interest in sCO_2 technology for power production, prompting more study and development in this field. Future research areas might involve doing detailed techno-economic evaluations of certain WH_2P applications to determine their cost-effectiveness and commercial feasibility. Developing and optimizing sCO_2 components and cycle designs for various waste heat sources[22]. Overall, Kacludis et al.'s research on sCO_2 WH_2P applications is noteworthy for its contribution to the advancement of this promising technology. While further study is needed to fully realize its potential, the insights and examples given provide a useful roadmap for future development and deployment of sCO_2 WH_2P systems in a variety of industrial sectors.

2.2 Absorption refrigeration system

Engineers conducted a thorough investigation of the functioning and use of the injection model in refrigeration systems, identifying possible benefits and overcoming potential hurdles. The injection model involves adding a refrigerant to the system in liquid, vapor, or two-phase form[23]. Any refrigerant in these conditions, according to the research, can be utilized for the injection procedure. A common form of injection is vapor injection. This method is commonly utilized because it increases the cooling and heating capacities of the compressor without needing a larger stroke volume change. Because of its simplicity, vapor injection is considered more practical and cost-effective. Pressure dips at the expansion valve at the higher stages of the cycle, as well as the design and chemical composition of the refrigerant mixture, all have a significant impact on the performance of the vapor injection refrigeration system. The Coefficient of Performance (COP), which assesses the system's efficiency, is an important metric. According to Xu et al.'s findings, infusing vapor into the refrigeration cycle can result in a significant boost in COP. The improvement over the baseline Vapor Compression Cycle (VCC) varies between 16% and 32%. This implies that the injection model, especially when vapor injection is utilized, has the potential to considerably enhance the overall efficiency of the refrigeration system. The injected vapor contributes to the improvement of thermodynamic processes within the cycle, resulting in improved performance and energy efficiency.

According to Mao and Zhou's experimental findings, including a flash tank in refrigeration cycles resulted in a 4.3% higher COP than a cycle with an IHX under identical operating circumstances. The flash tank most likely made a major contribution to the refrigeration system's overall efficiency. Gomri et al. conducted a second law study to compare single- and double-effect absorption refrigeration systems. The results revealed that the single-effect system had a maximum Coefficient of Performance (COP) of 0.79 in the 4-10°C evaporator temperature range. In contrast, the double-effect system demonstrated potential development, with a greater maximum COP of 1.42. Benramdane et al. employed an absorption refrigeration system that had three boilers and two absorbers, resulting in a greater overall COP. The precise arrangement of many boilers and absorbers is thought to have contributed to the absorption refrigeration system's superior performance. Weber et al. achieved chilled water temperatures as low as -1_2° C using a Fresnel collector with linear concentration. The Fresnel collector is a type of solar collector that focuses sunlight; its linear concentration design resulted in efficient cooling performance. Furthermore, the suggested system showed steady operation, indicating its appropriateness for cooling applications. Cimsit et al. suggest cascading a Vapor Compression Refrigeration (VCR) system with an Absorption Refrigeration Cycle (ARC) via a cascade heat exchanger.

This configuration, which combined a low-temperature cycle condenser (VCC) and a high-temperature cycle evaporator (ARC), produced a greater COP and the ability to achieve lower temperatures. Seara et al. tested a Combined Compression Absorption Refrigeration (CCAR) system, boosting the COP by 7.3% and the second-law efficiency by 3.3% by optimization. When compared to a vapor compression system, the CCAR system lowered power consumption by 50% while utilizing solar, geothermal, and waste heat resources. Han et al. demonstrated a hybrid absorption-compression refrigeration system using an ammonia-water binary combination, with compressors and evaporators shared by subsystems. Mehdi et al. designed a cascade absorption system to replace a traditional vapor compression system in natural gas liquefaction, achieving a COP of 0.48 while consuming 30% less electricity. Ocal et al. ($_2$011) investigated prospective teachers' comprehension and misunderstandings about global warming. This discovery is significant because educators play an important role in shaping future generations' understanding and attitudes regarding environmental issues. Despite having a basic understanding of global warming, many prospective instructors had misunderstandings about its causes, techniques, and impacts. Misconceptions regarding global warming include blaming it only on deforestation, ozone depletion, or industrial activities without considering the role of greenhouse gases. Participants mostly relied on informal media sources for information about global warming, such as television, radio, and the internet, underlining the risk of disinformation and wrong interpretation. Gender and department disparities: The study showed statistically significant differences in total exam outcomes across genders and academic departments, with female students and students from social studies departments outperforming their male peers. Inadequate environmental education: Because of limitations in their undergraduate education, prospective educators reported feeling unqualified to teach on global warming. The findings of Ocal et al. are consistent with previous studies stressing the prevalence of misunderstandings about global warming across various student groups (e.g., sterlind, 2005). The study contributes to previous research by focusing on prospective teachers and highlighting the importance of clearing up misconceptions in order to foster accurate and successful environmental education for future generations. The identified information sources and academic department differences are consistent with larger trends in scientific education and information consumption. The study is confined to a specific sample of potential teachers in Turkey, necessitating more research with a larger demography. The study focuses mostly on misunderstandings without delving into the root reasons and potential factors influencing student comprehension. Future study might focus on effective methods for addressing misunderstandings and enhancing accurate understanding of global warming

in teacher education programs[24], [25]. The role of various teaching approaches and information sources in building environmental knowledge and attitudes. Long-term effects of enhanced environmental education on prospective teachers' future teaching practices and student learning outcomes[26]. Overall, Ocal et al.'s study gives useful insights into prospective teachers' awareness and misconceptions about global warming in Turkey[27]. This research contributes to enhancing environmental literacy and promoting informed future generations by stressing the need for greater environmental education and effective solutions for overcoming misconceptions. Mahlman's 1997 work in Science, is a succinct yet significant addition to the field of climate change research[28]. It underlines the difficulty of projecting future climate patterns and the importance of ongoing studies to resolve uncertainty[29]. Climate change is caused by several variables, according to Mahlman, including greenhouse gas emissions, natural variability, and ocean-atmosphere interactions. He underlines the interplay of these elements, making it difficult to identify and quantify the precise impact of human-caused CO_2 emissions[30]. Model constraints: Despite great advances, climate models still have limits in describing complex Earth system processes. Uncertainties in model inputs, parameterizations, and future emission scenarios make precise projections of future climate change problematic[31]. Despite uncertainties, Mahlman admits the scientific consensus that human activities are warming the globe[32]. He gives a range of probable warming forecasts based on several model simulations and emission scenarios, emphasizing the likelihood of considerable temperature increases in the future decades. The report emphasizes the significance of continued research to improve climate models, minimize uncertainties, and deepen our understanding of climate change dynamics. This involves initiatives to improve data gathering and monitoring of climate parameters. Create more advanced climate models that better represent critical processes[28]. Conduct sensitivity assessments to investigate the impact of various factors on climate projections. Analyze and address uncertainties in model inputs and emission scenarios. Continued advancement of advanced climate models with higher resolution and modeling of major Earth system processes such as cloud formation, ocean circulation, and cryosphere dynamics. Efforts to reduce uncertainty in model inputs, particularly future emission scenarios, by the incorporation of insights from socioeconomic and policy studies. Climate models are used to inform vulnerability assessments at the regional and sectoral levels, as well as adaptation plans and mitigation measures. Improved communication strategies are being developed in order to better communicate the uncertainties and potential implications of climate change to policymakers, stakeholders, and the general public. Overall, Mahlman's 1997 paper remains an essential contribution to the current debate about climate change uncertainty[22]. It emphasizes the importance of ongoing study, greater understanding, and effective communication in preparing for the problems brought by climate change.

Chapter 3: Description of the model/System

3.1 Transcritical CO_2 Rankine Cycle with different layouts

The Rankine cycle freestanding models are specifically engineered to capture and utilize waste heat. The waste heat source was identified as the exhaust gas emitted by a 25-MWe-class gas turbine, with a mass flow rate of 69.8 kg/s at a temperature of 538 °C (811 °K). If the surrounding temperature was 15 degrees Celsius (288 K), a total of 40.9 MWth of waste heat would be generated.

For a simple setup, it is necessary to utilize a recuperator to maximize the turbine's input temperature and enhance the thermal efficiency of the cycle. However, increasing the turbine input temperature leads to a decrease in the efficiency of using waste heat from exhaust gases for heat recovery. The reason for this is that the recuperator elevates the temperature of the working fluid prior to its utilization. Therefore, it is crucial to maximize the net output power by integrating the thermal efficiency of the cycle with the efficiency of utilizing waste heat. The complete utilization of waste heat from a gas turbine is not achievable with a standard S-CO2 Rankine cycle due to the inherent trade-off between thermal efficiency and utilization efficiency.

The residual waste heat generated by the previous basic cycle can be harnessed by an additional S-CO2 Rankine cycle. The prior high-temperature (HT) loop (1-2-3H-4H5H-6H) and low-temperature (LT) loop (1-2-3L-4L-5L-6L), shown by the dashed line in Figure 3, were merged. A single pump was utilized to supply both loops, but the flow was divided into two separate streams following the pump. Each stream was directed through its respective heating loop and turbine. The portion indicated by x was directed to the HT loop, while the remaining amount (1-x) was directed to the LT loop. In the T-s diagram, the mass flow rate and heat capacity of the heat source remain constant for each unit mass of CO2. However, the slope of the heat source temperature varies depending on the mass flow rate of CO2 from the HT heater (x portion, 3L–4L) to the LT heater (1-x portion, 3H–4H). One can optimize the mass flow rates in both the high temperature (HT) and low temperature (LT) loops to maintain a constant pinch temperature, while simultaneously minimizing the temperature difference for heat transfer between the heat source and CO2.

Employing a split S-CO2 Rankine cycle is a supplementary approach to recuperate the residual waste heat from the preceding fundamental cycle. Despite the presence of a highly efficient recuperator, the temperature of the CO2 at state 3, which is located after the recuperator on the high-pressure side, is considerably lower than the temperature of the CO2 at state 5, which is located before the recuperator on the low-pressure side, in the previously described basic S-CO2 Rankine cycle. The reason for this is that the isobaric specific heat of CO2 is significantly greater on the high-pressure side compared to the low-pressure side. Consequently, the split S-CO2 Rankine cycle can utilize the excess waste heat from the basic S-CO2 Rankine cycle to compensate for the disparity in the isobaric specific heat of CO2 between the high-pressure and low-pressure sides, in order to achieve the maximum

temperature of CO2 after the recuperator (state 3). The section recovered from the residual heat of the enlarged working fluid, represented by x, is transferred to the recuperator once the pump is placed there. In order to utilize the unused waste heat from the HT heater, the portion that is not wasted (1-x) is directed towards the LT heater. The recuperator and the low-temperature heater elevate the temperature of the divided flow to an equal level after it passes through the pump. To minimize energy loss caused by the temperature difference between the fluxes, they are combined before reaching the HT heater (state 3). The expected pinch temperature, which is the minimum temperature difference required for heat transfer, was 10°C for the internal recuperator and 30°C for the exhaust gas-to-CO2 section. The T-s diagram depicts the relationship between the mass flow rate of CO2 from the high-temperature (HT) heater (x (1-x) section, 3e4) to the low-temperature (LT) heater (1-x portion, 2e3), which is indicated by the slope of the heat source temperature curve. To minimize the temperature difference for heat transfer in the heater and recuperator, the mass flow rates in the HT and LT loop can be varied while keeping the pinch temperature constant. It was hypothesized that carbon dioxide (CO2) would undergo condensation at a temperature of 20 degrees Celsius (293 K). Saturated liquid exits the condenser. Initially, it was believed that the upper pressure of the cycles would be 230 bar. Subsequent study was conducted to ascertain the impact of the cycles' elevated pressure on the net output power of the WHR.

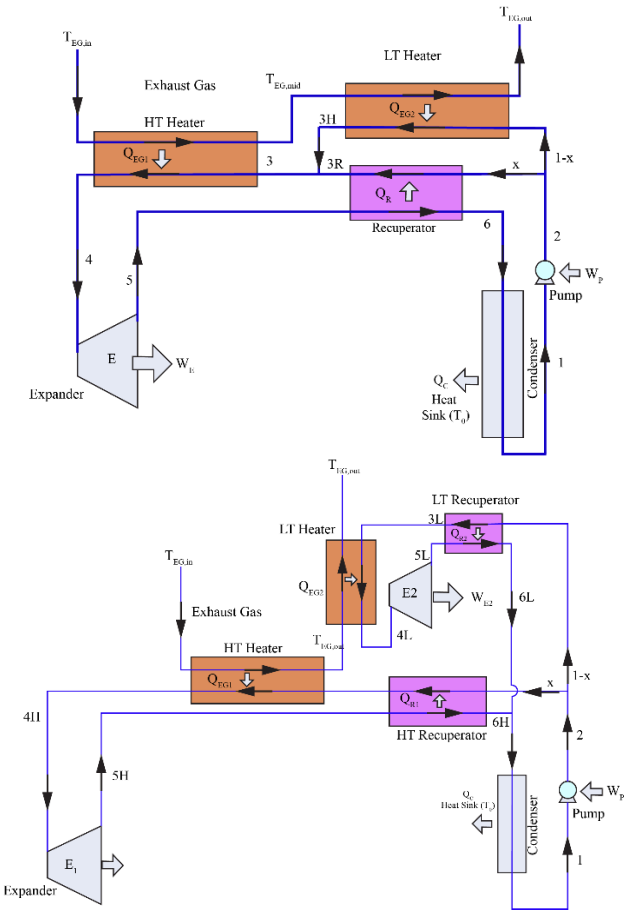

Figure 1: Schematic illustration of transcritical CO2 Rankine Cycle (a) Split Layout (b) Cascade Layout.

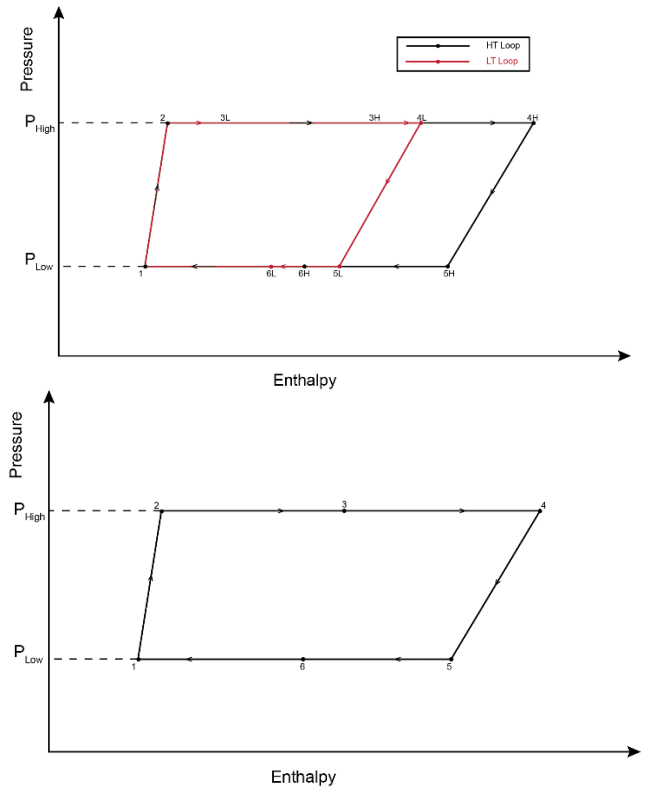

Figure 2: P-h diagram of (a) Split t-CO2 Rankine Cycle (b)Cascade t-CO2 Rankine Cycle

3.2 Absorption Refrigeration System

In order to enhance efficiency in terms of energy and exergy, the standard cascade absorption system is altered by incorporating a flash tank and an additional throttle valve (TV-IV) in the low-temperature cycle (LTC), as well as integrating a refrigerant heat exchanger (RHX) in the high-temperature cycle (HTC). HTC is considering two solutions, LiBr/H2O and NH3/H2O, for simulating the system. The LiBr/H2O solution mostly uses H2O as the refrigerant, while the NH3/H2O solution primarily uses NH3 as the refrigerant. The process of water evaporation occurs within the generator as a result of an external heat source heating a less concentrated solution of LiBr − H2O. Point 1: The concentrated LiBr − H2O solution in the generator remains after the water vapor has evaporated. At point 2, the water vapor from the generator is discharged from the condenser as a high-pressure liquid, having entered the condenser as a high-pressure liquid. The high-pressure water exits the cascade heat exchanger and enters the refrigerant heat exchanger (RHX), where it transfers heat to the low-temperature, low-pressure fluid at the exit point (point 4). Upon exiting the RHX, the high-temperature liquid undergoes subcooling at point 11 and proceeds to the throttle valve, where it is throttled (TV-I) to match the pressure of the cascade heat exchanger at point 3. The water undergoes evaporation within the cascade heat exchanger at point 4, transforming into

saturated vapor by absorbing heat from the refrigerant in the low-temperature circuit. The vapor enters the Regenerative Heat Exchanger (RHX), where it absorbs heat from the heated liquid. It then goes through the condenser and reaches point 12 of superheat. Afterward, the low-pressure water vapor enters the absorber, causing the LiBr - H2O solution to convert into a weak solution. The diluted solution is subsequently sent to the generator through point 5. After the water evaporates in the generator, the strong LiBr - H2O solution is returned to the absorber using a solution heat exchanger and TV-II. The high-temperature concentrated solution enters the Solution heat exchanger at point 8, transfers heat to the low-temperature dilute solution from points 6 to 7, and leaves the heat exchanger at point 9. The potent LiBr − H2O mixture is thereafter sent to the absorber through the throttle valve (TV-II) by means of throttling. However, when an NH3/H2O solution is employed, NH3 is used as the refrigerant instead of H2O. As a result, the solution flowing from the generator outlet to the absorber is diluted, while the solution flowing from the absorber to the generator is concentrated. Instead of utilizing an ideal VCC for the lower temperature circuit, a customized VCC incorporating a flash tank is utilized. The high-pressure superheated vapor of the LTC refrigerant enters the cascade heat exchanger at point 13. At point 14, heat is transferred to the LTC working fluid, causing it to undergo a phase change and become saturated liquid. The TV-III is thereafter employed to regulate it to an intermediate pressure (point 15). Upon entering the flash tank at point 19, the refrigerant undergoes a phase change and becomes a combination of liquid and vapor. The flash tank then separates the saturated vapor part and delivers it to the compressor. On the other hand, the lower part is restricted to the pressure of the evaporator at point 17, and the portion consisting of saturated liquid (point 16) is separated from it. The refrigerant, which is at a low pressure and low temperature, undergoes evaporation in the evaporator between points 17 and 18, resulting in the generation of a cooling effect. Following its departure from the evaporator, the saturated vapor is conveyed to the compressor, where it is merged with the intermediate pressure saturated vapor. At point 13, the mixture undergoes compression to generate a series of pressure changes in the heat exchanger, thus sustaining the cycle.

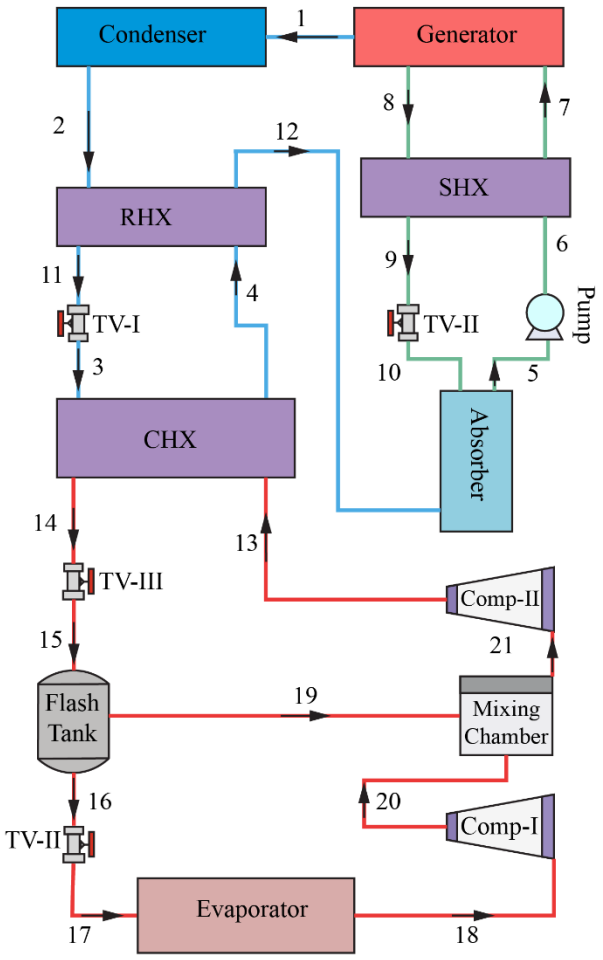

Figure 3: Schematic illustration of Advanced ARS.

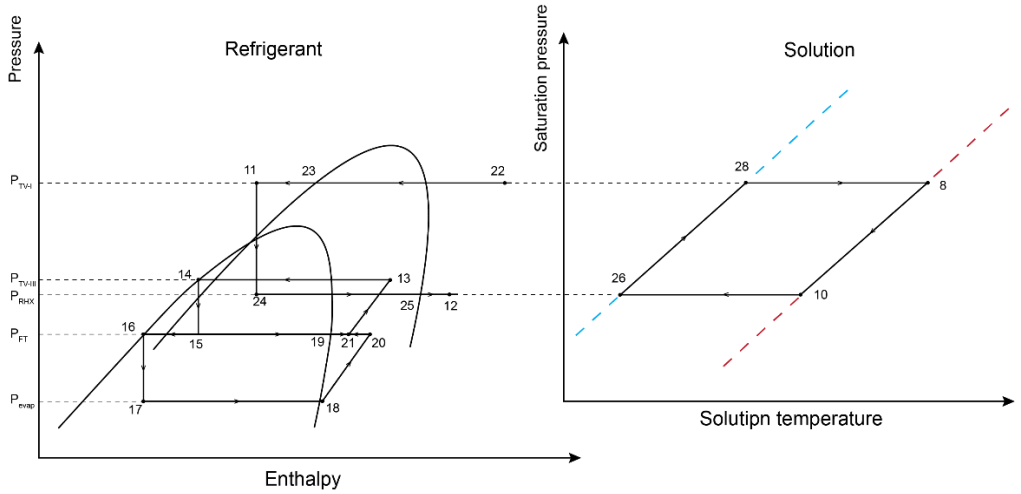

Figure 4: P-h diagram of the ARS along with the P-t diagram of the solution.

3.3 Proposed Novel Integrated System

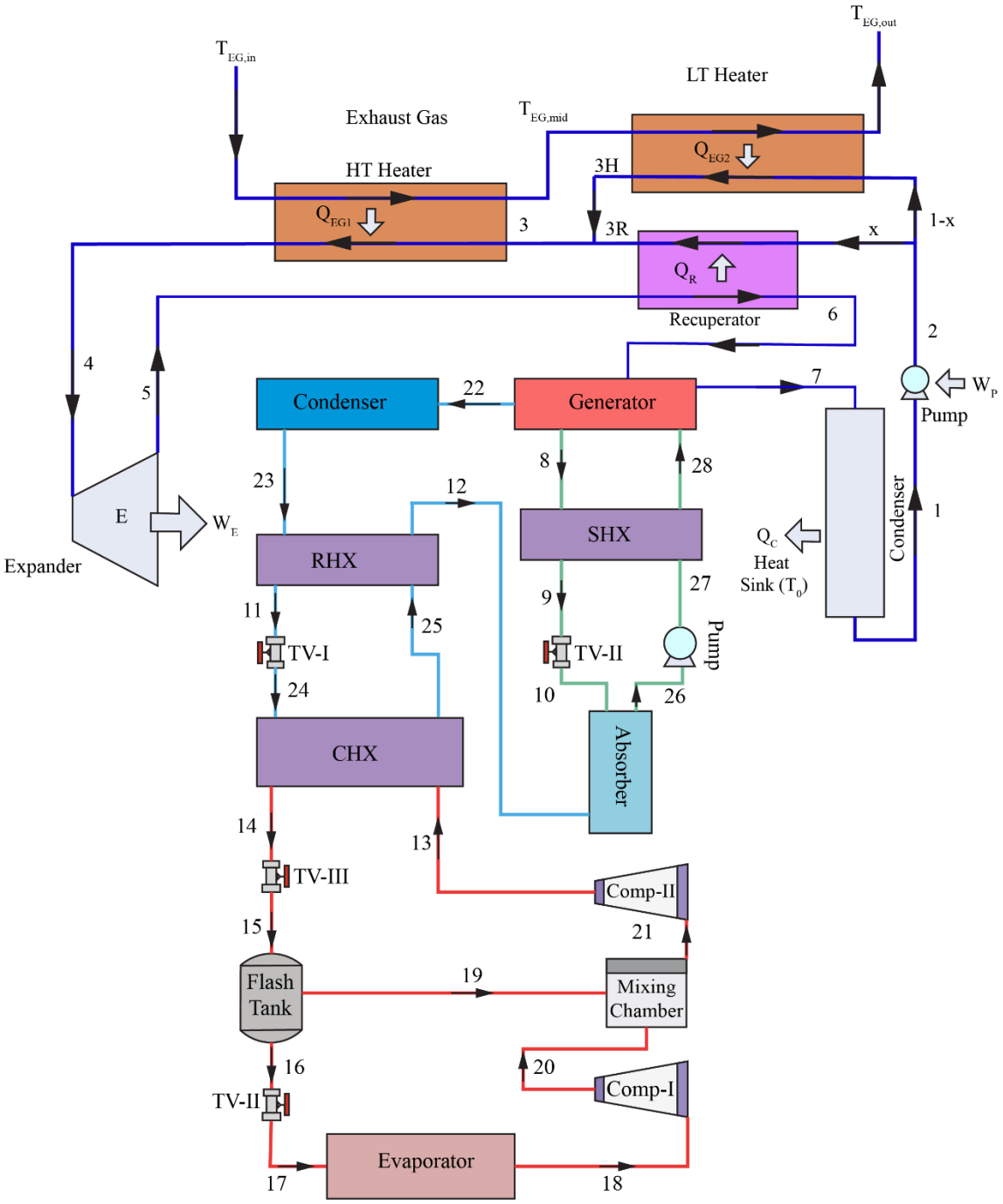

Figure 5: Split Transcritical CO2 cycle integrated with Novel Cascade Compression-Absorption refrigeration system ARS

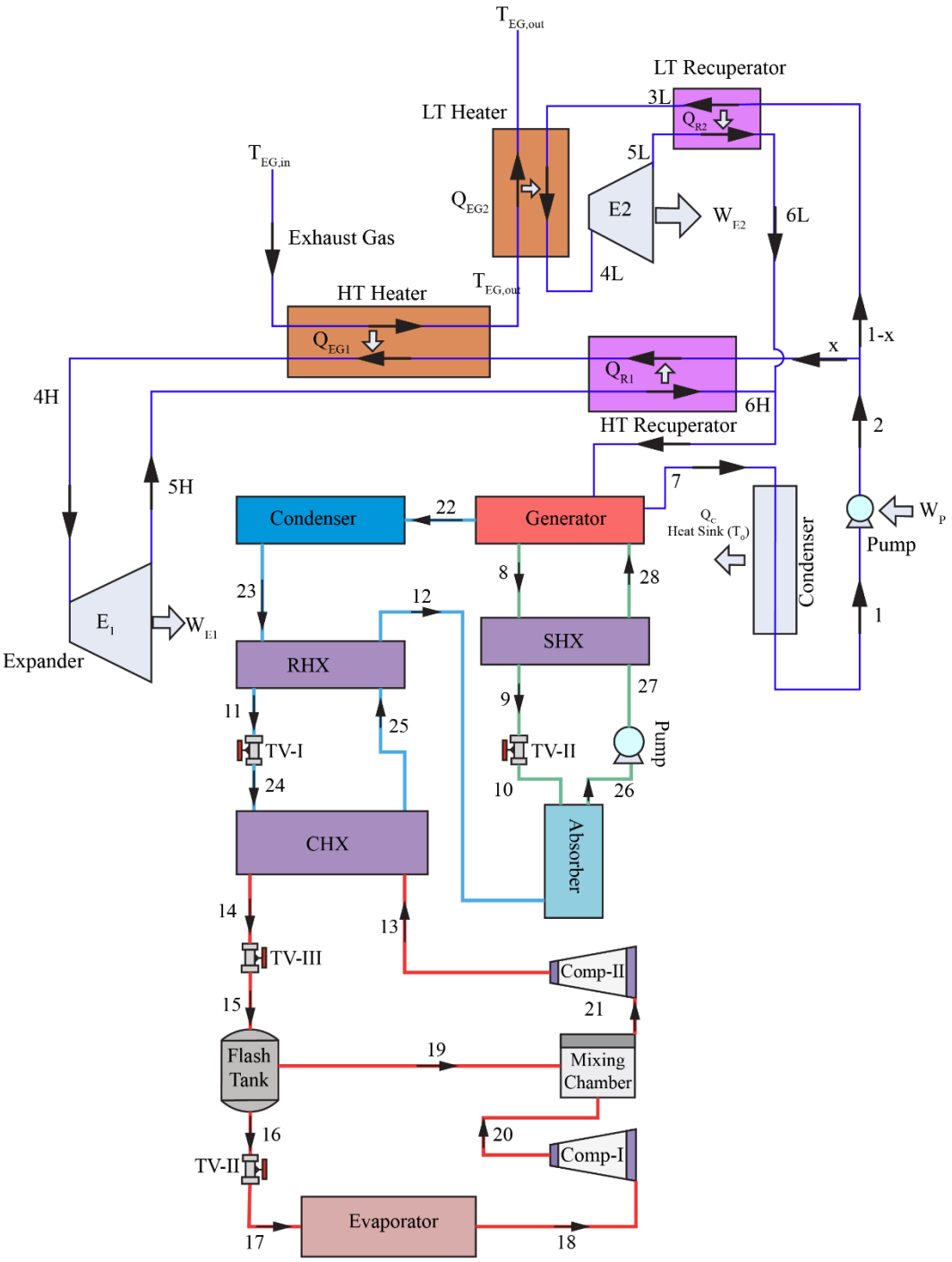

Figure 6: Cascade Transcritical CO2 cycle integrated with Novel Cascade Compression-Absorption refrigeration system ARS.

- Heat Source: Exhaust gas from a 25MWe gas turbine having a mass flow rate of 70kg/s and a temperature of 540 degree Celsius.
- Ambient temperature: 15 degrees Celsius.

- Waste Heat amount: 41 MWth.
- HTC: Single Absorption Refrigeration cycle implemented with a refrigerant heat exchanger.
- LTC: Vapor Compression Cycle integrated with a flash tank.
- Solution Used: NH_3/H_2O.

Refer to Figures 5-6 for a comprehensive grasp of the system configuration. This system features a cascade design, wherein it integrates two distinct absorption cycles that function at varying temperatures. The primary cycle, operating at high temperatures, produces chilled water for use in applications such as space cooling. Meanwhile, the secondary cycle, operating at lower temperatures, cools the generator stream of the high-temperature cycle. Both cycles utilize a lithium bromide-water (LiBr/H2O) solution as the working medium. The LiBr/H2O solution is heated, resulting in the evaporation of water. The heat can arise from several sources, such as waste heat generated by industrial processes and solar thermal collectors. The water vapor migrates to the condenser and undergoes condensation, transforming into a liquid with elevated pressure. The high-pressure liquid water transmits thermal energy to the low-pressure fluid when it enters the cascade heat exchanger, therefore reducing its temperature. The high-pressure liquid undergoes expansion through the throttle valve, resulting in a decrease in both pressure and temperature. The low-pressure liquid water absorbs thermal energy from the refrigerant in the low-temperature circuit, such as ammonia or CO2, causing it to undergo evaporation. The goal of this water is to be used for space cooling or other applications. Subsequently, the water vapor is sent back to the RHX where it absorbs thermal energy from the heated liquid in the condenser. The highly heated water vapor from the regenerative heat exchanger (RHX) enters the absorber and is assimilated by the concentrated lithium bromide/water solution, leading to the formation of a diluted solution. The diluted solution is reintroduced into the generator to complete the cycle. A solution of LiBr diluted with water absorbs heat from a low-temperature source, resulting in the evaporation of the water. A highly concentrated solution of LiBr/H2O has the ability to absorb water vapor in a manner that is comparable to the high-temperature cycle. The feeble solution is introduced into the generator of the low-temperature cycle. The generator heats the diluted solution, causing the release of water vapor into the condenser of the low-temperature cycle. The water vapor undergoes condensation, transforming into a liquid under high pressure. This liquid then moves to the cascade heat exchanger to be cooled during the high-temperature cycle. A solution heat exchanger is a device used to transfer heat between two fluids or solutions. By preheating the dilute LiBr/H2O solution before to entering the generator, the efficiency is enhanced. The Throttle Valve (TV-II) reduces the pressure of the concentrated LiBr/H2O solution prior to its arrival to the absorber, hence enhancing absorption. The implementation of cascading architecture enables the effective usage of waste heat and energy sources of low quality. Additionally, the generator's heat input and flow rates can be adjusted to meet different cooling needs. LiBr/H2O is a safe and non-flammable working fluid. Nevertheless, it requires meticulous observation of multiple elements and operating circumstances.

The superheated refrigerant vapor from the low-temperature cycle (LTC) is directed into the cascade heat exchanger at point 13. It undergoes cooling and condensation, transforming into

saturated liquid (at point 14), by transferring heat to the hot liquid in the high-temperature cycle. The liquid refrigerant undergoes partial expansion via a throttle valve (TV-III) in order to attain an intermediate pressure at point 15. This process results in a combination of liquid and gaseous states. The refrigerant mixture is introduced into a flash tank. The tank evaporates the high-pressure vapor component (point 19), which is thereafter directed directly to the compressor. The residual low-pressure liquid (point 16) is discharged from the bottom of the flash tank and then brought down to the pressure of the evaporator (point 17). This novel adaptation of the Vapor Compression Cycle (VCC) incorporates a low-pressure flash tank to improve the efficiency of the system. The refrigerant, functioning under low pressure and temperature conditions, extracts heat from an external source in the evaporator (points 17-18), undergoing a phase change from liquid to vapor. Interestingly, the vapor stream that is produced passes through a process of separation inside the flash tank. Point 19, which is the high-pressure part, deviates from the usual compression path and connects directly to the compressor inlet. This process eliminates the need for energy-intensive compression of the low-pressure liquid fraction, resulting in a significant improvement in overall efficiency. Simultaneously, the vapor with low pressure (point 18) begins its separate path and eventually combines with the high-pressure flow at the entrance of the compressor. Subsequently, both streams are compressed to the pressure of the cascade heat exchanger, which is denoted as point 13, so concluding the cycle. This ingenious architectural design utilizes the abundant high-pressure vapor that is easily accessible, optimizing its role in the cooling process and minimizing the need for excessive compression labor. In addition, the throttling valve, located at point 15, has a vital function in precisely regulating the intermediate pressure and enhancing the efficiency of the system. By precisely adjusting this parameter, it is possible to control the flow rates and thermodynamic features of the refrigerant streams in order to optimize efficiency and increase cooling capacity. Essentially, this improved VCC utilizes a low-pressure flash tank and optimized throttling valve to avoid wasted compression effort and open up new possibilities for improved system performance. This makes it a strong candidate for future refrigeration applications.

Through the analysis of existing literature, it was determined that the cascade and split configurations of the top cycle show promise as potential sources of waste heat for powering modern refrigeration systems. The advanced refrigeration system that was discovered is far more efficient than the typical cascade refrigeration system. As a result, two distinct integrations can be suggested: i) Cascade Rankine cycle with Advanced Recuperative System (ARS) ii) Implement a Rankine cycle with an Auxiliary Reheat System (ARS) to divide the cycle into multiple stages. In both of these setups, the excess heat from the top cycle's stream was removed prior to its passage through the condenser. The condenser operates within a temperature range of 60 to 70 degrees Celsius, corresponding to the chosen pressure ratio of 23 MPa (upper pressure) and 5.7 MPa (lower pressure). The thermal energy from the upper cycle is directed towards the generator of the lower cycle, where the residual heat is subsequently harnessed to drive the other components of the lower cycle.

The system modeling is implemented using the Python programming language and may be visualized in Figure 3. The 'Coolprop' function library is required for thermodynamic

modeling of the proposed innovative system. The library has the capability to calculate various state point values based on the component, fluid stream, and other predetermined criteria. The algorithm first executes and calculates the various state point values for the top cycle. The condenser temperature is set as a constant, determined from previous modeling research. The waste heat, which has a temperature of 10 degrees Celsius, is directed into the generator inlet of the bottom cycle.

The state points in different cycle components are determined based on the heat generated by the generator. This is done using library functions. Finally, the result functions are defined based on thermodynamic principles to evaluate the overall performance of the system, which is represented by the COP of the bottom cooling system. In order to verify that the suggested innovative system is working within appropriate parameters, the individual top and bottom cycles were verified using information from previous studies. The results of these validations are reported in the following sections.

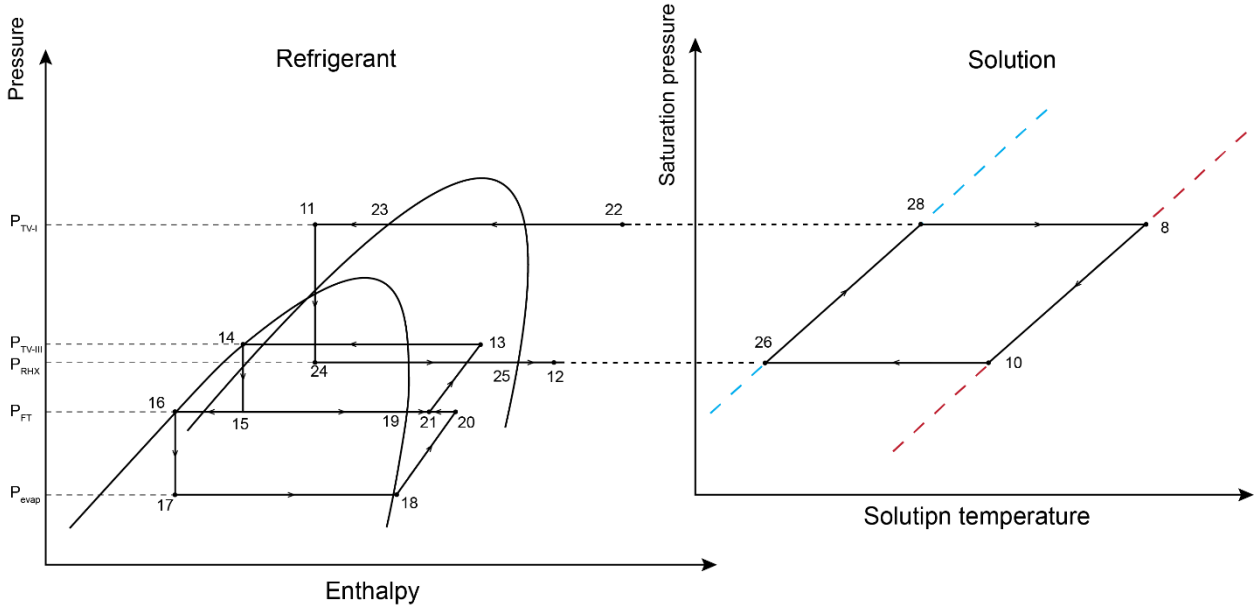

Figure 7: P-h diagram of the bottom ARS along with the P-t diagram of the solution.

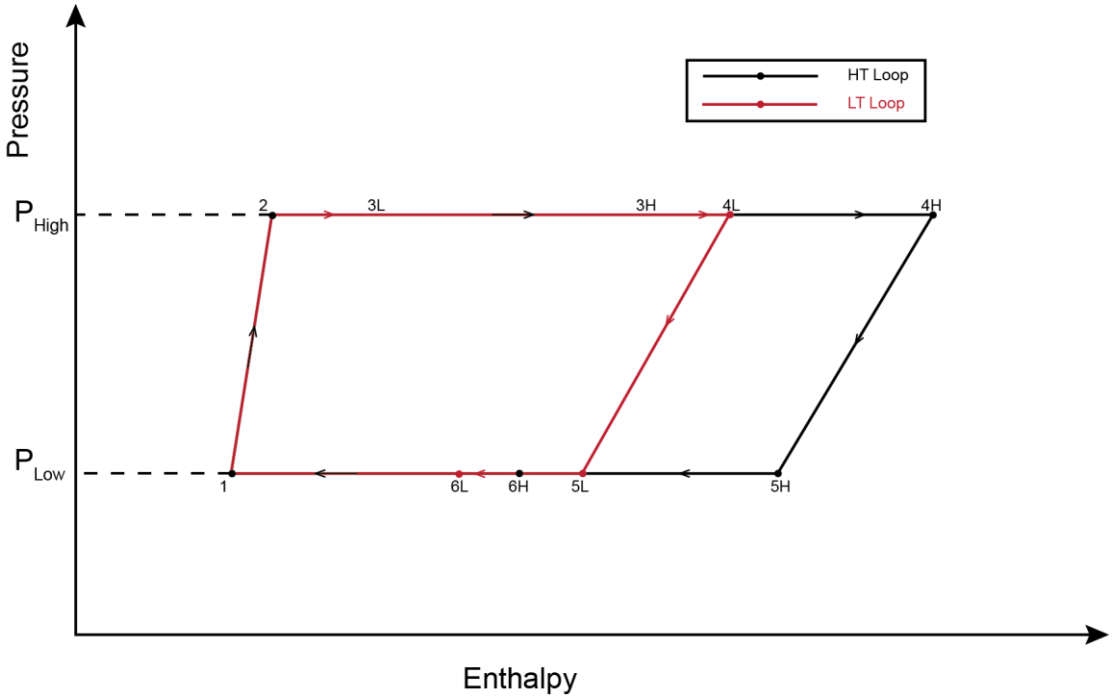

Figure 8: P-h diagram of top Split t-CO2 Rankine Cycle.

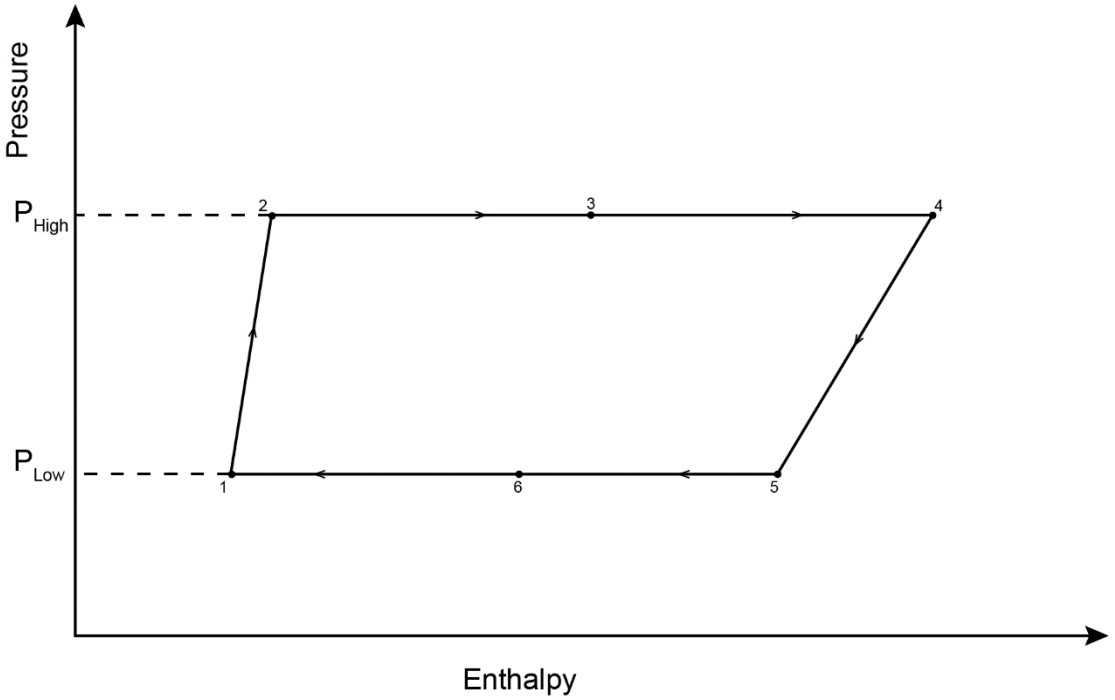

Figure 9: P-h diagram of top Cascade t-CO2 Rankine Cycle.

Chapter 4: Computational Methodology

4. Thermodynamic Modeling

4.1 Assumptions

To streamline the simulations, the following assumptions are included.

- No heat exchange is taken into account with the surroundings beyond what has been mentioned.
- The simulation is conducted in a state of equilibrium.
- The pressure decreases insignificantly in the pipe and heat exchangers.
- Fluid characteristics at the output of the mixing chamber are supposed to remain constant across the whole cross-section after complete mixing.
- The solutions exiting the absorber and generator are in a state of equilibrium.
- Throttle valves undergo a continuous process of constant enthalpy, while the pump undergoes an isentropic process.
- The refrigerant that leaves the evaporator and the condenser is in a state of saturation.
- When NH3/H2O is utilized in the absorption cycle, the vapor exiting the generator is regarded as 100% NH3. Conversely, when LiBr/H2O is employed in the absorption cycle, the vapor departing the generator is considered 100% H2O.
- The solutions that leave the generator and absorber are in a state of saturation.
- The amount of effort performed by the pump in the absorption cycle is believed to be insignificant.

4.2 Energy Analysis

By utilizing the principles of conservation, one can employ equations for mass, energy, and exergy balance to calculate the different thermodynamic parameters at different points in time within each component of the corresponding cycles. These computations eventually ascertain the performance of the cycle. To apply mass, energy, and exergy balancing, one can use the components as a control volume.

The principle of mass balance allows us to apply continuity equations to each component of the corresponding cycles. The mass balance equation is represented by the following expression:

$$\sum \dot{m}_i = \sum \dot{m}_e \tag{1}$$

From the definition of COP,

$$COP = \frac{Desired\ Output}{Work\ Input} \tag{2}$$

Three top cycle setups were created using Python programming. The study examines three specific configurations: simple, cascade, and split. The mathematical equations are presented in tabular form below:

Three configurations of the top cycle were configured using python codes. The configurations considered in the study are namely, simple, cascade and split. The mathematical equations are

tabulated below:

Table 2: Governing equations for energy analysis.

Cycle Configuration/Parameter	Component/Parameter	Equation
Energy Analysis		
Simple	Pump	$\eta_p = \frac{h_{2,s} - h_1}{h_2 - h_1}$
Simple	Pump	$\dot{w}_p^+ = \dot{m}_{CO2}(h_2 - h_1)$
Simple	Turbine	$n_T = \frac{h_4 - h_5}{h_{4,s} - h_5}$
Simple	Turbine	$\dot{w}_E^- = \dot{m}_{CO2}(h_4 - h_5)$
Simple	Recuperator	$\varepsilon_R = \frac{\dot{m}_{CO2}(h_5 - h_6)}{\dot{Q}_{max}} = \frac{\dot{m}_{CO2}(h_3 - h_2)}{\dot{Q}_{max}}$
Simple	Rate of max heat exchange	$\dot{Q}_{max} = \dot{m}_{CO2}(h_5 - h_6)$
Simple	Heat exchange in heater	$\dot{Q}_H^+ = \dot{m}_{EG}\left(h_{EG,in} - h_{EG,out}\right) = \dot{m}_{CO2}(h_4 - h_3)$
Simple	Condenser	$\dot{Q}_c^- = \dot{m}_{CO2}(h_6 - h_1)$
Simple	Cycle thermal efficiency	$\eta_{cyc} = \frac{\dot{w}_E^- - \dot{w}_p^+}{\dot{Q}_H^+}$
Simple	Heat recovery efficiency	$\eta_{HR} = \frac{\dot{Q}_H^+}{\dot{Q}_{H,max}^+} = \frac{\dot{m}_w(h_{in} - h_{out})}{\dot{m}_w(h_{in} - h_0)} = \frac{h_{in} - h_{out}}{h_{in} - h_0}$
Simple	System efficiency	$\eta_{sys} = \frac{\dot{w}_E^- - W_P^+}{\dot{Q}_{H,max}^+} = \eta_{HR} n_{cyc}$

Bottom Cycle

Mass conservation at CCFT:

$\dot{m}_{13} = \dot{m}_{14} = \dot{m}_{15}$

$\dot{m}_{16} = \dot{m}_{17} = \dot{m}_{18}$

$\dot{m}_{19} + \dot{m}_{20} = \dot{m}_{21}$

Mass conservation at ACR:

$\dot{m}_{22} = \dot{m}_{23} = \dot{m}_{11} = \dot{m}_{24} = \dot{m}_{25} = \dot{m}_{12}$

$\dot{m}_{22} + \dot{m}_{8} = \dot{m}_{28}$

$\dot{m}_{26} = \dot{m}_{27} = \dot{m}_{28}$

$\dot{m}_{8} = \dot{m}_{9} = \dot{m}_{10}$

For $\mathrm{LiBr/H_2O}$ solution, mass flow rates of the solution:

$$CR = \frac{\dot{m}_8}{\dot{m}_{22}} = \frac{X_{28}}{X_8 - X_{28}}$$

The circulation ratio (CR) is defined as the ratio of the mass flow rate of the strong solution to that of the refrigerant. The mass flow rates of the NH_3/H_2O solution are given in reference [59].

$$CR = \frac{\dot{m}_{28}}{\dot{m}_{22}} = \frac{1 - X_8}{X_{28} - X_8}$$

Energy balance equation for evaporator:

$$\dot{Q}_{\text{evp}} = \dot{m}_{18} \times (h_{18} - h_{17})$$

Energy balance equation for compressor:

$$\dot{W}_{\text{comp}} = \dot{m}_{18} \times \frac{h_{20s} - h_{18}}{\eta_s} + \dot{m}_{13} \times \frac{h_{13s} - h_{21}}{\eta_s}$$

Energy balance equation for the mixing chamber:

$$m_{21} \times h_{21} = m_{19} \times h_{19} + m_{20} \times h_{20}$$

Where, η_s is the isentropic efficiency of the compressors. The compressors are assumed to be well designed making its isentropic efficiency between 0.75 and 0.85.

Energy balance equation for cascade hear exchanger:

$$\dot{Q}_{CHX} = \dot{m}_{13} \times (h_{13} - h_{14}) = \dot{m}_{24} \times (h_{25} - h_{24})$$

Energy balance equation for refrigerant heat exchanger:

$$T_{11} = T_{23} - \varepsilon_{RHX} \times (T_{23} - T_{25})$$

$$h_{12} = h_{25} + (h_{23} - h_{11})$$

Where, ε_{RHX} is the effectiveness of the refrigerant heat exchanger. Energy balance equation for solution heat exchanger:

$$T_9 = \varepsilon_{SHX} \times T_{27} + (1 - \varepsilon_{SHX}) \times T_8$$

$$h_{28} = h_{27} + (h_8 - h_9) \times \frac{\dot{m}_8}{\dot{m}_{28}}$$

Energy balance equation for absorber:

$$\dot{Q}_{abs} = \dot{m}_{12} \times h_{12} + \dot{m}_{10} \times h_{10} - \dot{m}_{26} \times h_{26}$$

Energy balance equation for generator:

$$\dot{Q}_{\text{gen}} = \dot{m}_{22} \times h_{22} + \dot{m}_8 \times h_8 - \dot{m}_{28} \times h_{28}$$

Energy balance equation for condenser:

$$\dot{Q}_{\text{cond}} = \dot{m}_{22} \times (h_{22} - h_{23})$$

The performance of the proposed refrigeration system can be calculated by evaluating the COP from the perspective of first law of thermodynamics.

$$COP = \frac{\dot{Q}_{\text{evp}}}{\dot{Q}_{\text{gen}} + \dot{W}_{\text{comp}}}$$

4.3 Exergy analysis

t-CO_2 Rankine Cycle

Table 3: Governing equations for exergy analysis.

Cycle Configuration/Parameter	**Component/Parameter**	**Equation**
Exergy Analysis		
Fluid Stream	Exergy	$\dot{E} = \dot{m}k = \dot{m}[h - h_0 - T_0(s - s_0)]$
Exhaust Gas	Exergy Transfer	$\dot{E}^{+}_{H,EG} = \dot{m}_{EG}[h_{in} - h_{Out} - T_0(S_{in} - S_{out})]$
Maximum Allowable	Exergy Transfer	$\dot{E}^{+}_{H,max} = \dot{m}_{EG}[h_{in} - h_O - T_0(S_{in} - S_0)]$
Ideal gas		$h_{in} - h_0 = C_p(T_{in} - T_0)$
Ideal gas		$s_{in} - s_0 = c_p ln\frac{T_{in}}{T_0} - r\, ln\frac{P_{in}}{P_0}$

	Exergy Transfer	$\dot{E}^{+}_{H,max} = \dot{m}_{EG} C_P \left[(T_{in} - T_0) - T_0 ln \frac{T_{in}}{T_0} \right]$
Second Law	Heat recovery efficiency	$\eta_{HR,II} = \frac{\dot{E}^{+}_{H}}{\dot{E}^{+}_{H,max}} = \frac{\dot{m}_w (k_{in} - k_{0ut})}{\dot{m}_w (k_{in} - k_0)} = \frac{k_{in} - k_{out}}{k_{in} - k_0}$
CO_2 stream	Exergy	$\dot{E}_{CO2} = \dot{m}_{CO2} k = \dot{m}_{CO2} [h - h_0 - T_0 (s - s_0)]$
Exergy Balance		$\dot{E}^{+} - \dot{E}^{-} = \dot{L}$
Pump	Exergy Loss	$\dot{L}_P = \dot{E}_P{}^{+} - \dot{m}_{CO2} (k_2 - k_1)$
Turbine	Exergy Loss	$\dot{L}_T = \dot{m}_{C02} (k_4 - K_5) - \dot{E}^{-}_{T}$
Recuperator	Exergy Loss	$\dot{L}_R = \dot{m}_{CO2} (k_5 - k_6) - \dot{m}_{CO2} (k_3 - k_2)$
Heater	Exergy Loss	$\dot{L}_H = \dot{E}^{+}_{H} - \dot{m}_{CO2} (k_4 - k_3)$
Condenser	Exergy Loss	$\dot{L}_C = \dot{m}_{CO2} (k_6 - k_1)$
Cycle	Second Law efficiency	$\eta_{cyc,II} = \frac{\dot{E}^{-}_{T} - \dot{E}^{+}_{p}}{\dot{E}^{+}_{H}}$
System	Second Law Efficiency	$\eta_{sys,II} = \frac{\dot{E}^{-}_{T} - \dot{E}^{+}_{p}}{\dot{E}^{+}_{H,max}} = n_{HR,II} n_{CyC,II}$

Bottom Advanced ARS

Exergy can be stated as the maximum work potential of an energy stream corresponding to the surrounding environment. In a steady-state controlled volume system, the exergy balance equation is expressed as:

$$\dot{E}_{D,i} = \sum (\dot{m}_{\text{in}} \times ex_{\text{in}}) - \sum (\dot{m}_{\text{out}} \times ex_{\text{out}}) + \sum \dot{Q} \times \left(1 - \frac{T_o}{T}\right)_{\text{in}}$$

Where, the term 'ex' represents the exergy of an energy stream in the steady-state controlled volumed system, $\dot{E}_D$ represents the exergy destruction rate in the system, and T_0 is the average temperature of the environment. The exergy of an energy stream can be stated in the following equation:

$$ex_i = h_i - h_o - T_o \times (s_i - s_o)$$

Exergy destruction of each component of the system is evaluated in the following manner:

For evaporator:

$$\dot{E}_{D,evp} = \dot{m}_{18} \times (ex_{17} - ex_{18}) + \dot{Q}_{evp} \times \left(1 - \frac{T_o}{T_{evp}}\right)$$

Compressor:

$$\dot{E}_{D.\,\text{comp}} = \left(\dot{m}_{18} \times (s_{20} - s_{18}) + \dot{m}_{13} \times (s_{13} - s_{21})\right) \times T_o$$

Throttle process:

$$\dot{E}_{D,TV} = \left(\dot{m}_{14} \times (s_{15} - s_{14}) + \dot{m}_{16} \times (s_{17} - s_{17}) + \dot{m}_{24} \times (s_{24} - s_{11})\right) \times T_o$$

Cascade heat exchanger:

$$\dot{E}_{D,CHX} = \left(\dot{m}_{14} \times (s_{14} - s_{13}) + \dot{m}_{24} \times (s_{25} - s_{24})\right) \times T_o$$

Absorber:

$$\dot{E}_{D,abs} = \dot{m}_{25} \times ex_{12} + \dot{m}_{10} \times ex_{10} - \dot{m}_{10} \times ex_{10} - \dot{Q}_{abs} \times \left(1 - \frac{T_o}{T_{abs}}\right)$$

Refrigerant heat exchanger:

$$\dot{E}_{D,RHX} = \left(\dot{m}_{23} \times (s_{11} - s_{23}) + \dot{m}_{25} \times (s_{12} - s_{25})\right) \times T_o$$

Solution heat exchanger:

$$\dot{E}_{D,SHX} = \left(\dot{m}_{27} \times (s_{28} - s_{27}) + \dot{m}_{9} \times (s_{9} - s_{8})\right) \times T_o$$

Generator:

$$\dot{E}_{D,gen} = \dot{m}_{28} \times ex_{28} - \dot{m}_{8} \times ex_{8} - \dot{m}_{22} \times ex_{22} + \dot{Q}_{gen} \times \left(1 - \frac{T_o}{T_{gen}}\right)$$

So, the total exergy destruction rate can be calculated as:

$$\dot{E}_{D,\,\text{total}} = \dot{E}_{D,\,\text{evp}} + \dot{E}_{D,\,\text{comp}} + \dot{E}_{D,TV} + \dot{E}_{D,CHX} + \dot{E}_{D,abs} + \dot{E}_{D,RHX} + \dot{E}_{D,SHX}$$

$$+\dot{E}_{D,gen}$$

Additionally, the exergetic efficiency of the overall system can be calculated by:

$$\eta_{II} = \frac{\dot{Q}_{evp} \times \left|1 - \frac{T_o}{T_{evp}}\right|}{\dot{Q}_{\text{gen}} \times \left[1 - \frac{T_o}{T_{\text{gen}}}\right] + \dot{W}_{\text{comp}}}$$

4.4 Fixed Parameters and System flow-chart

A mathematical model has been developed using the 'PyCharm Edu' coding platform. This model incorporates mass, energy, and exergy balance equations, which are described in detail in section 3.2 Energy Analysis. 3.3 Exergy analysis. The characteristics of the working fluid (transcritical carbon dioxide), and refrigerant are obtained using the built-in library functions in Python. The characteristics of the solution are calculated using empirical equations. The simulation begins by initializing with a predetermined set of operating settings, as described in the table below.

Table 4: Fixed data used in the simulation

Parameters	Values
Mass flow rate of exhaust gas	69.8 kg/s
Turbine exhaust gas inlet temperature	538 ℃
Turbine exhaust gas middle temperature	289 ℃
Turbine exhaust gas outlet temperature	73.8 ℃
Turbine inlet temperature (Split)	308 ℃
Turbine inlet temperature (Cascade)	538 ℃
Ambient temperature, T_0	25 ℃
Ambient pressure, P_0	101.325 kPa
Condenser temperature (t-CO_2)	23 ℃
Cycle Low Pressure	6.2 MPa
Effectiveness of Pump	0.8
Effectiveness of Turbine	0.85
Effectiveness of Recuperator	0.9
Evaporator Temperature	-20 ℃
Absorber Temperature	35 ℃
Condenser Temperature	35 ℃
Evaporator Temperature (HTC)	5 ℃
Effectiveness of Solution Heat Exchanger (SHX)	0.9
Effectiveness of Refrigerant Heat Exchanger (RHX)	0.7
Generator hot stream temperature	10 ℃
Generator cold stream temperature	3 ℃
Pressure Ratio	4
Cycle High Pressure	24.8 MPa

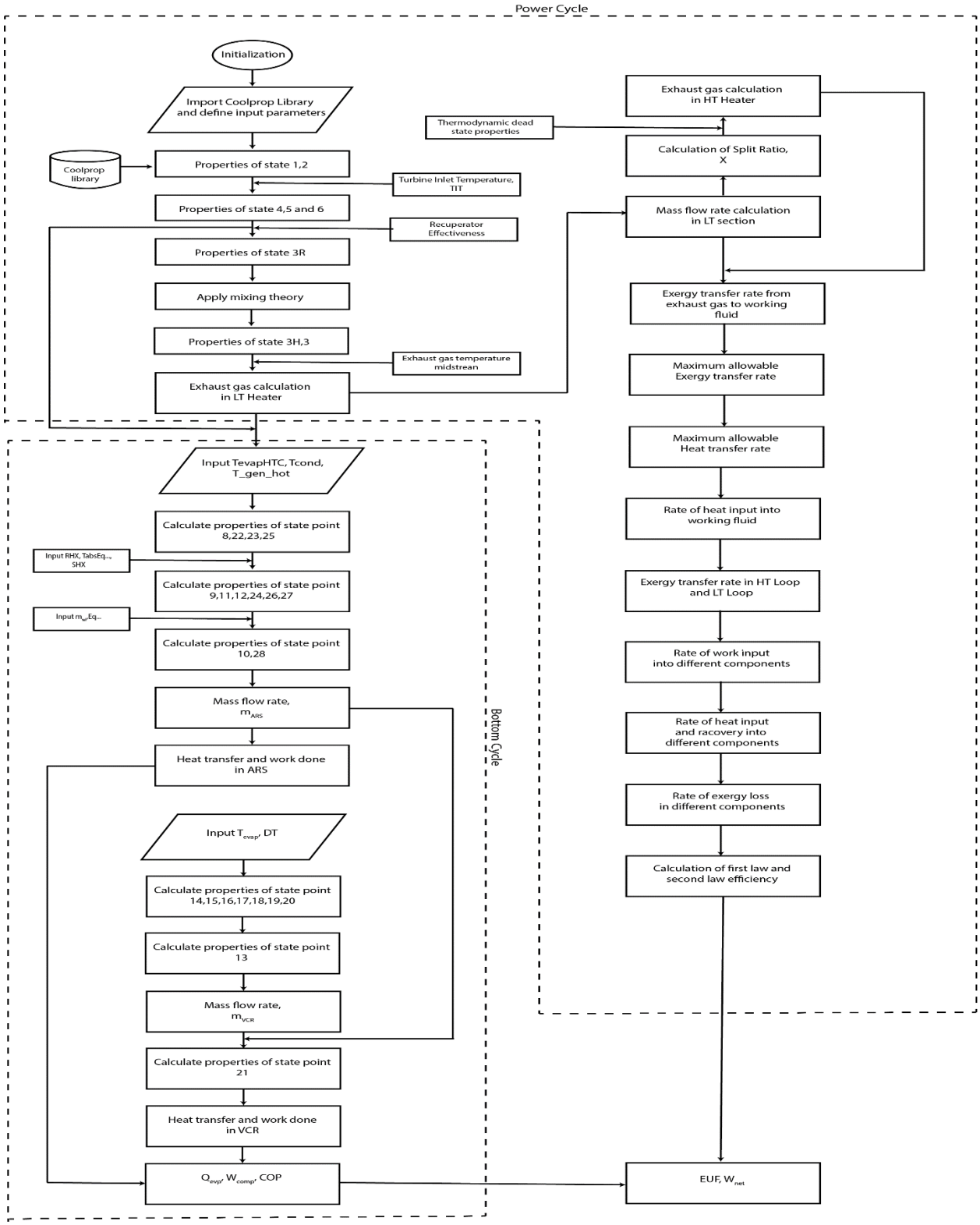

Figure 10: Framework of the mathematical model for the proposed system

4.5 Model Validation

Due to the unique nature of our proposed systems, they cannot be compared or validated against any existing studies. Nevertheless, as our systems are designed to incorporate independent setups of Rankine cycles with a sophisticated ARS system, it is possible to verify the conventional stand-alone cycles and the advanced refrigeration cycles using the existing research. Our validation process will involve testing transcritical Carbon dioxide Rankine cycles, specifically the split and cascade configurations, that incorporate advanced compression-ARS combined with a flash tank and a reheater. These configurations will be compared to existing research to ensure their accuracy and effectiveness.

The validation of transcritical Carbon dioxide Rankine cycles was conducted based on a study by Kim et al. The publication presents the findings of the investigation, which are summarized below. The generated model is also compared with the findings for validation purposes.

Table 5: State point validation for different layouts of the Rankine cycle.

Parameters	Present Work	Kim et. Al.	Relative diff. (%)
Split			
Condenser Exergy Loss, L_C (kW)	442	454	2.64
Pump Exergy Loss, L_P (kW)	533	545	2.20
Recuperator Exergy Loss, L_R (kW)	1067	1090	2.11
HT heater Exergy Loss, L_{HT} (kW)	1160	1188	2.35
LT heater Exergy Loss, L_{LT} (kW)	1159	1147	-1.04
Turbine Exergy Loss, L_E (kW)	1864	1885	1.11
$\eta cycle, II$	0.652	0.636	-2.45
$\eta HR, II$	0.960	0.980	2.04
$\eta sys, II$	0.598	0.614	2.60
Total exergy loss	6213	6356	2.25
Cascade			
HT Condenser Exergy Loss, L_C (kW)	374	366	2.1
HT Pump Exergy Loss, L_P (kW)	305	296	2.7
HT Recuperator Exergy Loss, L_R (kW)	2814	2836	2.3
HT heater Exergy Loss, L_{HT} (kW)	527	532	1.91
LT heater Exergy Loss, L_{LT} (kW)	1070	1089	2.82
HT Turbine Exergy Loss, L_E (kW)	110	104	2.03

$\eta cycle, II$	0.584	0.533	2.51
$\eta HR, II$	0.953	0.949	2.33
$\eta sys, II$	0.556	0.547	2.09
HT Total exergy loss	5090	5102	1.02
LT Condenser Exergy Loss, L_C (kW)	212	209	1.11
LT Pump Exergy Loss, L_P (kW)	118	117	0.15
LT Recuperator Exergy Loss, L_R (kW)	695	693	0.20
LT heater Exergy Loss, L_{HT} (kW)	654	648	1.32
LT Turbine Exergy Loss, L_E (kW)	118	121	1.01
LT Total Exergy Loss	1789	1764	2.43

The model was evaluated using a diverse range of 'Turbine inlet temperature' values to calculate the associated cycle and system efficiency. The results were compared to the findings of the reference paper to validate the model.

The table displays errors of less than 3% for various parameters. An error occurred as a result of utilizing disparate libraries for numerical simulation. The Engineering Equation Solver (EES) Programme was utilized in our research to calculate various state points in different layouts/configurations of the Rankine cycle. This was achieved by employing specific equations that were defined for each computation. In our situation, we utilized the PyCharm Edu coding environment to determine the properties of the working fluid using the included library function 'coolprop'.

Table 6: State point validaion for the ARS.

Parameters	**Present Work ($LiBr/H_2O$)**	**Ref. ($LiBr/H_2O$)**	**Present Work (NH_3/H_2O)**	**Ref. (NH_3/H_2O)**	**Relative diff (%)**	**Relative diff (%)**
Generator Load, $\dot{Q}gen$ (kW)	3093	3093	17.07	16.77	0.00	-1.79
Absorber Load, $\dot{Q}abs$ (kW)	2942	2943	15.62	15.33	0.03	-1.89
Condenser Load, $\dot{Q}cond$ (kW)	2506	2506	11.45	11.43	0.00	-0.17
Evaporator Load, $\dot{Q}evp$ (kW)	2355	2355	10.00	10.00	0.00	0.00

The bottom cycle (advanced compression-ARS combined with a flash tank and a reheater) is validated against the paper of Md Walid et. Al.

The provided graphs are validation graphs for a thermodynamic system, focusing on various efficiencies and performance metrics.

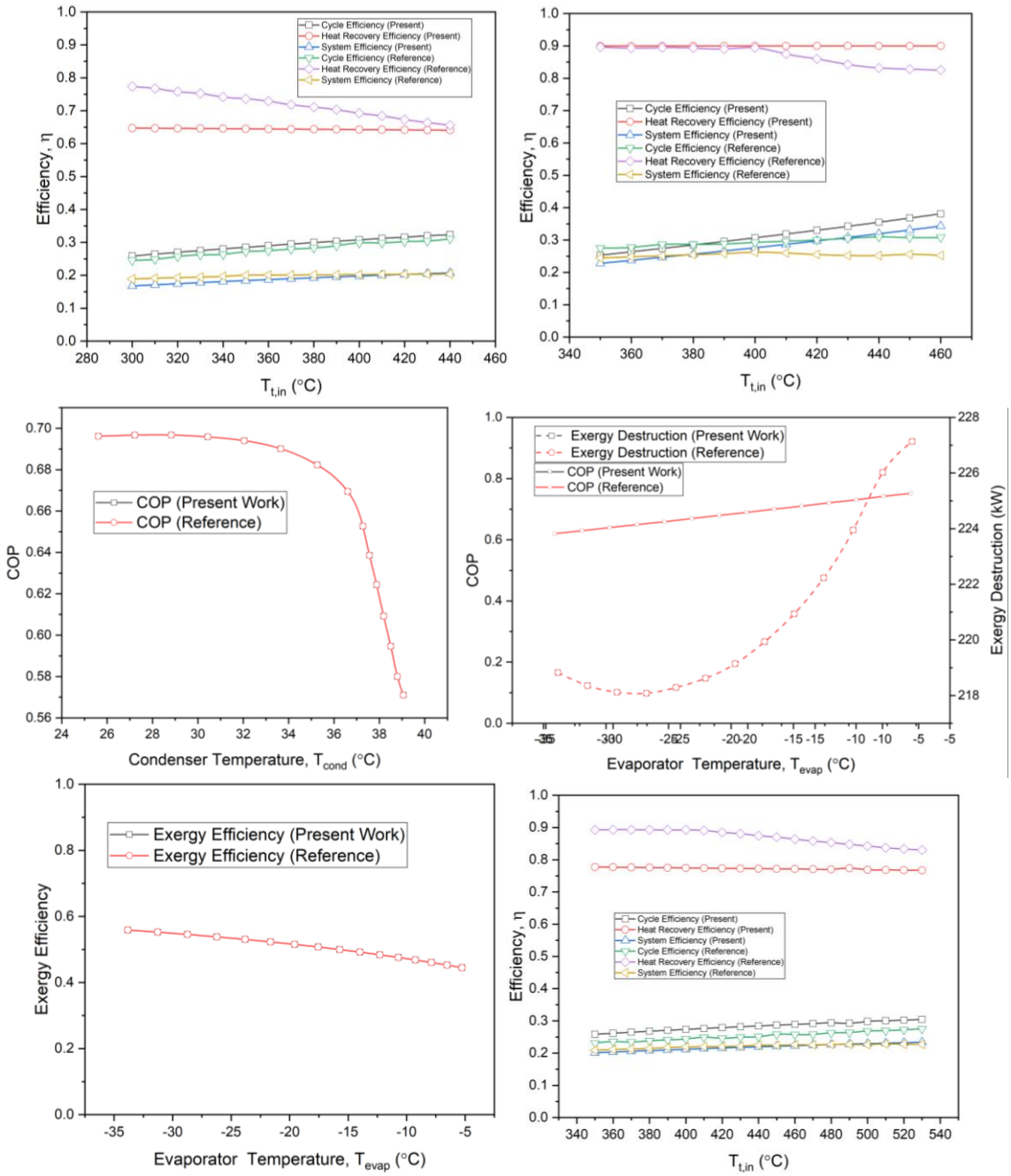

Figure 10: Parametric validation of different parameters.

The first graph, "Efficiency vs. $T_{t,in}$ (Present and Reference)", compares different efficiencies (Cycle Efficiency, Heat Recovery Efficiency, and System Efficiency) for both the present and reference systems across a range of inlet temperatures ($T_{t,in}$). Cycle Efficiency represents the efficiency of the cycle alone, Heat Recovery Efficiency indicates the efficiency of the heat recovery process, and System Efficiency combines both cycle and heat recovery efficiencies to give an overall measure of system performance.

The second graph, also "Efficiency vs. $T_{t,in}$, extends the temperature range, providing a broader view of how the same efficiencies for both present and reference systems behave

over a different set of temperatures. This extended range allows for a more comprehensive analysis of the system's performance under varying conditions.

The third graph, "COP vs. Condenser Temperature (T_{cond}), compares the Coefficient of Performance (COP) of the present work and the reference system across various condenser temperatures. COP is a crucial metric in thermodynamic systems, indicating the efficiency of the system in converting energy input into useful work or output.

The fourth graph, "COP and Exergy Destruction vs. Evaporator Temperature (T_{evap}) presents a dual-axis plot where COP and Exergy Destruction (in kilowatts) for both the present work and the reference system are plotted against the evaporator temperature. Exergy Destruction measures the loss of useful energy during the process, while COP again provides insight into the system's performance efficiency.

The fifth graph, "Exergy Efficiency vs. Evaporator Temperature (T_{evap}), shows the exergy efficiency of the present work and the reference system as a function of evaporator temperature. Exergy Efficiency indicates how effectively the system converts available energy into useful work, with higher values representing better performance.

These graphs collectively validate the performance of a thermodynamic system, comparing current results with reference data across different operational parameters, helping to identify improvements and optimizations in the system's design and operation. State Point parameters of the bottom advanced Absorption Refrigeration System:

Table 7: State point parameters of the novel system.

Stream	T(°C)	P(kPa)	h(kJkg^{-1})	s (kJ kg^{-1}K^{-1})	x (%)	Mass Flow Rate (kg/s)
1	75	5.629	2641	8.584	-	0.1365
2	35	5.629	146.6	0.5051	-	0.1365
3	5	0.8725	58.8	0.2121	-	0.1365
4	5	0.8725	2510	9.025	55.28	0.1365
5	35	0.8725	85.31	0.2114	55.28	2.932
6	35	5.629	85.31	0.2114	55.28	2.932
7	69.32	5.629	153	0.4274	55.28	2.932
8	75	5.629	176	0.4391	57.98	2.796
9	39	5.629	105	0.2238	57.98	2.796
10	39	0.8725	105	0.2238	57.98	2.796
11	14	5.629	58.8	0.2099	-	0.1365
12	31.85	0.8725	2560	9.317	-	0.1365
13	25.06	2666	561.8	2.272	-	1
14	10	2666	227.1	1.093	-	1
15	-5.837	1742	227.1	1.103	-	0.8809
16	-5.837	1742	185.4	0.947	-	0.8809
17	-20	1138	185.4	0.9539	-	0.8809
18	-20	1138	536.4	2.34	-	0.8809

19	-5.837	1742	534.9	2.254	-	0.1191
20	8.754	1742	562.5	2.354	-	0.8809
21	-5.195	1742	536.2	2.259	-	1

Chapter 5: Results and Discussions

After verifying the thermodynamic model, a comparative thermal study was conducted on the proposed tCO2(split)+ARS system and the tCO2(cascade)+ARS system. The studies rely on multiple performance metrics, including COP, generator load (Q˙_gen), compressor load (W˙_comp), exergetic efficiency (η_II), and total exergy destruction (E˙_(D,total)). The functioning parameters of the system include four changeable variables: Turbine Inlet temperature (TIT), evaporator temperature (Tevp), condenser temperature (Tcond), and absorber temperature (Tabs).

5.1 Thermodynamic Performance Analysis

A Python Programme is utilized to simulate the suggested models. The refrigerant pair R41-LiBr/H2O has been chosen to assess and compare its thermal performance. The justification for the selection is based on its environmentally beneficial attributes and wide availability. This characteristic improves its compatibility for usage in circuits with lower temperatures, sometimes known as low temperature circuits (LTC). Prior research has also indicated the use of this coolant because of its exceptional efficiency in low-temperature uses. The thermodynamic state parameters of the proposed innovative systems are presented in the following tables, taking into account the specified boundary conditions given in the relevant tables.

Table: Thermodynamic state point properties of the Split t-CO_2+ARS at TIT = 308°C, T_{evp} = -20°C, T_{abs} = 35°C, T_{cond} = 35°C

State Point	T (°C)	x (%)	$\dot{m}$ (kg s^{-1})	h (kJ kg^{-1})	s (kJ kg^{-1} K^{-1})	P (kPa)	Point Exergy(kW)
1	35	-	0.1498	146	0.5031	5.583	0.08838
2	4	-	0.1498	55.23	0.1998	0.805	0.02952
3	4	-	0.1498	2508	9.054	0.805	-27.83
4	35	0.5588	2.029	87.36	0.2072	0.805	61.1
5	35	0.5588	2.029	87.36	0.2072	52.32	61.1
6	66.6	0.5588	2.029	151.2	0.4048	52.32	71.19
7	111	0.5588	2.029	244.1	0.6605	52.32	105
8	130	0.58	1.955	288.1	0.7365	52.32	143
9	85.6	0.58	1.955	197.1	0.4984	52.32	103.7
10	85.6	0.58	1.955	197.1	0.4984	5.583	103.7
11	130	-	0.07402	2741	7.825	52.32	30.6
12	82.6	-	0.07402	345.3	1.105	52.32	1.528
13	35	-	0.07402	345.3	1.15	5.583	0.5226
14	80.1	-	0.07578	2643	8.614	5.583	6.092
15	80.1	0.6034	1.879	196	0.4503	5.583	124.7
16	48.5	0.6034	1.879	135.7	0.2711	5.583	111.6
17	48.5	0.6034	1.879	135.7	0.2711	0.805	111.6
18	13.3	-	0.1498	55.23	0.1975	5.583	0.1336
19	52.4	-	0.1498	2599	9.356	0.805	-27.71
20	-27.1	-	0.9633	535.7	2.385	897.9	155.6

21	48.5	-	0.9633	605.3	2.418	2589	213.2
22	9	-	0.9633	223.9	1.082	2589	229.2
23	-31.3	-	0.9633	215.3	1.089	779.2	219.2
24	241.7	-	1.712	355.2	1.667	779.2	333.7
25	245.9	-	1.712	360	1.67	897.9	340.4
26	245.9	-	0.7485	134.4	0.7525	897.9	184.7
27	243	-	0.7485	134.4	0.7532	814.2	184.5
28	243	-	0.7485	535.2	2.403	814.2	116.5
29	241.7	-	0.7485	533.3	2.404	779.2	114.8

Table: Thermodynamic state point properties of the Cascade t-CO_2+ARS at TIT = 538°C, T_{evp} = -20°C, T_{abs} = 35°C, T_{cond} = 35°C

State Point	T (°C)	x (%)	$\dot{m}$ (kg s^{-1})	h (kJ kg^{-1})	s (kJ kg^{-1} K^{-1})	P (kPa)	Point Exergy(kW)
1	35	-	0.1498	146	0.5031	5.583	0.08838
2	4	-	0.1498	55.23	0.1998	0.805	0.02952
3	4	-	0.1498	2508	9.054	0.805	-27.83
4	35	0.5588	2.967	87.36	0.2072	0.805	89.34
5	35	0.5588	2.967	87.36	0.2072	42.2	89.34
6	67.2	0.5588	2.967	152.6	0.4088	42.2	104.6
7	340.2	0.5588	1.881	152.6	0.4088	42.2	66.32
8	340.2	0.5588	1.881	152.6	0.4088	5.583	66.32
9	340.2	0.5588	1.085	152.6	0.4088	42.2	38.25
10	111.8	0.5588	1.085	245.8	0.6651	42.2	56.61
11	130	0.6059	1.001	295.3	0.7074	42.2	89.04
12	81.7	0.6059	1.001	200.3	0.4572	42.2	68.62
13	81.7	0.6059	1.001	200.3	0.4572	5.583	68.62
14	349.9	0.5885	2.817	182.9	0.4425	5.583	156.5
15	130	-	0.08432	2720	7.926	42.2	30.57
16	77.3	-	0.08432	323.1	1.042	42.2	1.447
17	35	-	0.08432	323.1	1.078	5.583	0.5344
18	74.8	-	0.06548	2634	8.586	5.583	5.239
19	74.8	0.579	1.816	174.9	0.4377	5.583	88.97
20	44.6	0.5885	2.817	120	0.2538	5.583	137.8
21	44.6	0.5885	2.817	120	0.2538	0.805	137.8
22	13.3	-	0.1498	55.23	0.1975	5.583	0.1336
23	52.4	-	0.1498	2599	9.356	0.805	-27.71
24	-27.1	-	0.9633	535.7	2.385	897.9	155.6
25	48.5	-	0.9633	605.3	2.418	2589	213.2
26	9	-	0.9633	223.9	1.082	2589	229.2
27	-31.3	-	0.9633	215.3	1.089	779.2	219.2
28	-31.3	-	1.712	355.2	1.667	779.2	333.7
25	-27.1	-	1.712	360	1.67	897.9	340.4
26	-27.1	-	0.7485	134.4	0.7525	897.9	184.7

27	-30	-	0.7485	134.4	0.7532	814.2	184.5
28	-30	-	0.7485	535.2	2.403	814.2	116.5
29	-31.3	-	0.7485	533.3	2.404	779.2	114.8

5.2 Effect of Turbin Inlet Temperature ($T_{t,IT}$)

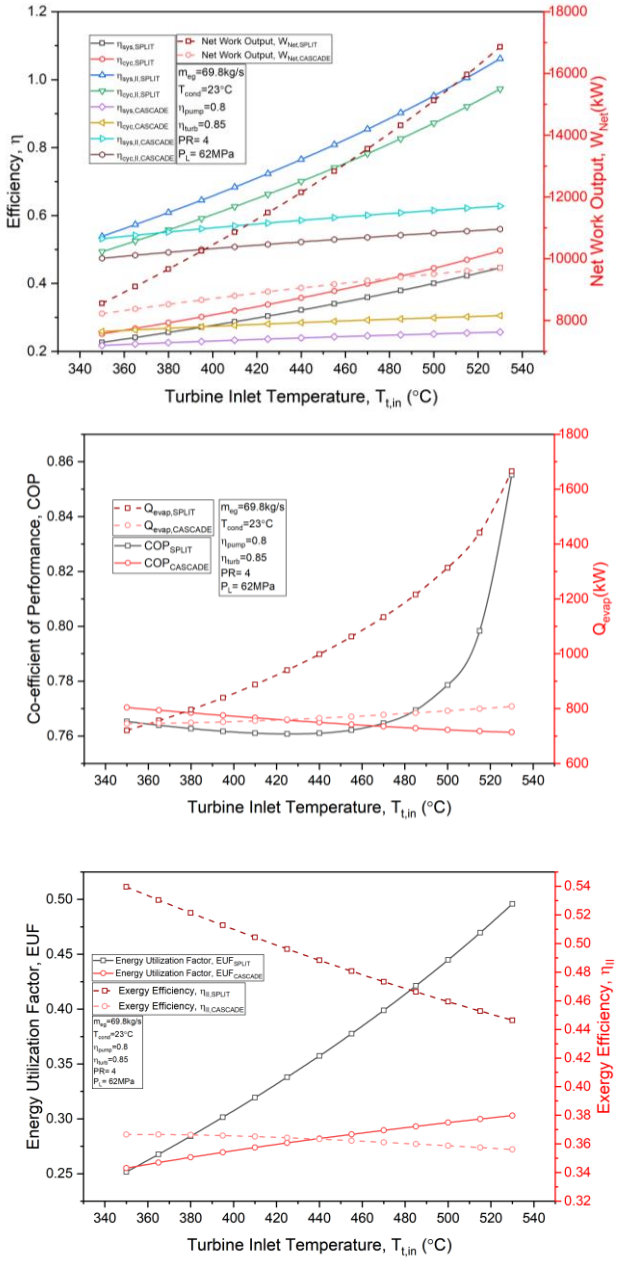

Figure 11: Effect of Turbin Inlet Temperature on performance parameters.

The initial graph provides a comprehensive comparison of the thermal efficiency and exergy efficiency of the split cycle and cascade cycle. The comparison is conducted over a temperature range spanning from 350 to 530 degrees Celsius. The x-axis depicts the Turbine Inlet Temperature (Tt,int), while the y-axis on the left displays the efficiency (η) and the y-

axis on the right indicates the net-work output (WNet) measured in kilowatts (kW). The graph compares various efficiency indicators. The efficiency of the first and second laws are graphed for both the system and cycle in the split and cascade cycles. The metrics consist of $\eta_{sys,SPLIT}$ (System Efficiency for the split cycle), ηcyc,SPLIT (Cycle Efficiency for the split cycle), ηsys,II,SPLIT (Second Law System Efficiency for the split cycle), and $\eta_{cyc,II,SPLIT}$ (Second Law Cycle Efficiency for the split cycle). The efficiencies associated with the cascade cycle are denoted as ηsys,CASCADE, ηcyc,CASCADE, ηsys,II, and ηcyc,II,CASCADE. In addition, the graph compares the network outputs (WNet,SPLIT and WNet,CASCADE) for both cycles. In general, the split cycle has superior efficiency compared to the cascade cycle within the specified temperature range. The split cycle's greater performance can be linked to the cascade cycle's need for an extra turbine and heater, which increases complexity and decreases overall efficiency. The split cycle demonstrates superior performance in terms of the Coefficient of Performance (COP) as a result of its optimized operating parameters. The coefficient of performance (COP) is a fundamental measure in thermodynamic systems that quantifies the system's efficiency in transforming energy input into usable output. The split cycle demonstrates a better coefficient of performance (COP) than the cascade cycle, indicating a more efficient utilization of energy input. The improved performance can be credited to the split cycle's streamlined architecture, which reduces energy losses and maximizes energy conversion processes. The split cycle's higher coefficient of performance (COP) is achieved by optimizing parameters such as mass flow rate, condenser temperature, pump efficiency, and turbine efficiency. This ensures that the system runs as close as possible to its theoretical maximum efficiency. Due to its higher coefficient of performance (COP), the split cycle also offers a more effective cooling effect. A higher coefficient of performance (COP) in thermodynamic systems indicates a more efficient cooling process, where a greater proportion of the energy input is turned into cooling output rather than being dissipated as waste heat. The split cycle's improved cooling efficiency allows it to attain accurate cooling temperatures more effectively, making it ideal for applications that require precise temperature control and huge cooling capacity. This benefit is especially notable in industrial and commercial cooling applications where energy efficiency and cooling performance are crucial considerations. In these cases, the split cycle is recommended over the cascade cycle due to its greater cooling capabilities and ability to maintain high efficiency. The overall second law efficiency of both systems decreases as the turbine inlet temperatures vary, whereas the energy utilization factor shows a positive trend.

5.3 Effect of Cycle Low Pressure (P_L)

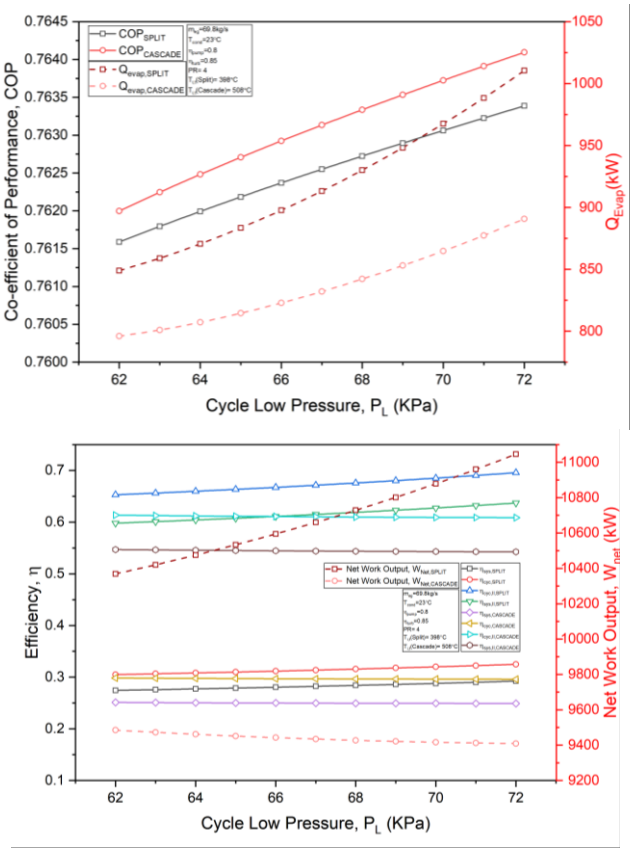

Figure 12: Effect of Cycle Low Pressure on fitness parameters.

The data in Figure demonstrates a clear positive association between the minimum pressure (Pmin) and the net-work. This means that when Pmin increases, the net-work also increases. The relationship arises from the fact that an increase in the minimum pressure (Pmin) causes a greater loss of enthalpy in both the t-CO2 High-Pressure Turbine (HPT) and Low-Pressure Turbine (LPT), leading to an overall enhancement in the total work output of the t-CO2 cycle. This increase in W_net also leads to a higher thermal efficiency. As the minimum pressure (Pmin) rises, the mass flow rate through the turbines and heaters of t-CO2 decreases, resulting in a reduction in the overall exergy destruction of the top cycle. Within the cascade refrigeration cycle, the coefficient of performance (COP) and the cooling load (Qevp) both exhibit an increase as the minimum pressure rises. This phenomena occurs when the split ratio varies in reaction to the minimum pressure, leading to an increase in the mass flow rate across the coolers.

.

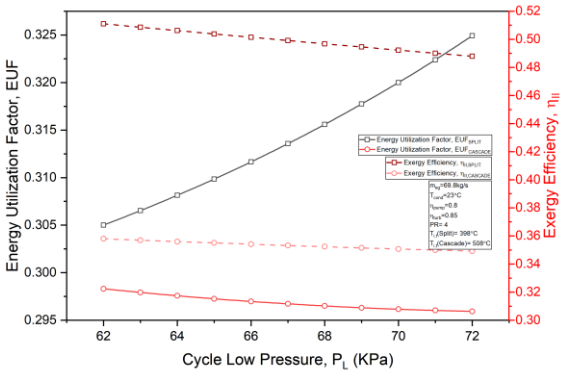

Figure 13: Effect of Cycle Low Pressure on fitness parameters. (contd.)

Consequently, the generator experiences a higher amount of heat (Qgen), leading to an increase in both the coefficient of performance (COP) and the heat output (Qevp). An increase in the minimum pressure (Pmin) causes a decrease in the input temperature of the generator. Consequently, the drop in the generator's operating temperature (Tgen) results in a decrease in both the coefficient of performance (COP) and the evaporator heat transfer rate (Qevp). The Efficiency Utilisation Factor (EUF) of the combined cycle increases within a defined range of increments in Pmin, which is between 6.2 MPa and 7.3 MPa. This phenomenon arises due to the opposing rates at which work is performed and the cooling load increases and the rate at which the cooling load decreases. Nevertheless, after the pressure above 7 MPa, the cooling load experiences a substantial decline, resulting in a reduction in the Energy Use Factor (EUF). Moreover, when the turbines exert greater effort, there is a discernible enhancement in the second law efficiency.

5.3 Effect of Pressure Ratio (PR)

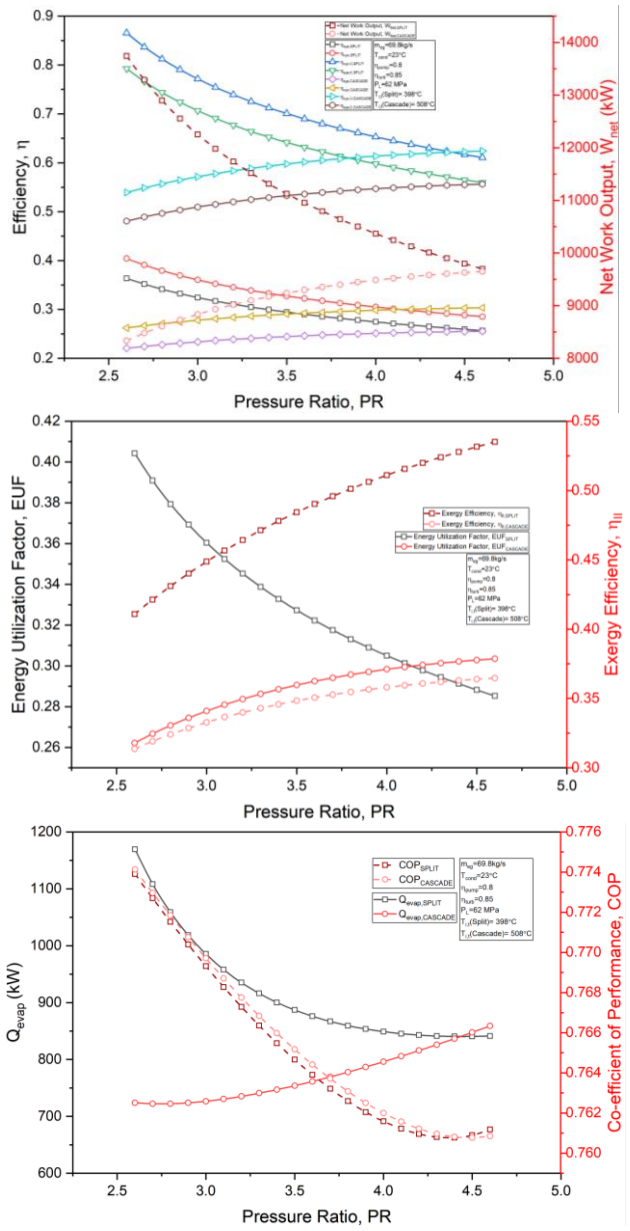

Figure 14: Effect of Pressure Ratio (PR).

The data depicted in the images illustrate a direct correlation between the pressure ratio (PR) and the net-work, suggesting that an increase in the pressure ratio results in a corresponding increase in the net-work. The correlation between the increase in pressure ratio (PR) and the rise in enthalpy loss in both the t-CO2 high-pressure turbine (HPT) and low-pressure turbine (LPT) results in an augmentation of the overall work output of the t-CO2 cycle. The rise in W_net also leads to an increase in thermal efficiency. However, when the pressure ratio (PR) increases, the mass flow rate of t-CO2 decreases, leading to a decrease in the overall exergy destruction of the upper cycle. In the cascade refrigeration cycle, an increase in the pressure ratio results in a higher generator inlet temperature (state point 6), which in turn leads to an increase in both the cooling load (Qevp) and the coefficient of performance (COP). However,

the drop in mass flow rate leads to a reduction in both the generator's workload and the cooling requirements, as seen in the Figure. Furthermore, the increase in W_net exceeds the decrease in Qevp as PR expands. The Efficiency Utilisation Factor (EUF) increases when the turbine inlet temperature (TIT) rises, as seen in the Figure. By raising the turbine inlet temperature (TIT), the accompanying increase in net work output (W_net) can compensate for the decrease in exhaust energy (Exd). Consequently, the exergy efficiency also rises with an increase in the pressure ratio (PR).

5.4 Effect of Absorber Temperature (T_{aba})

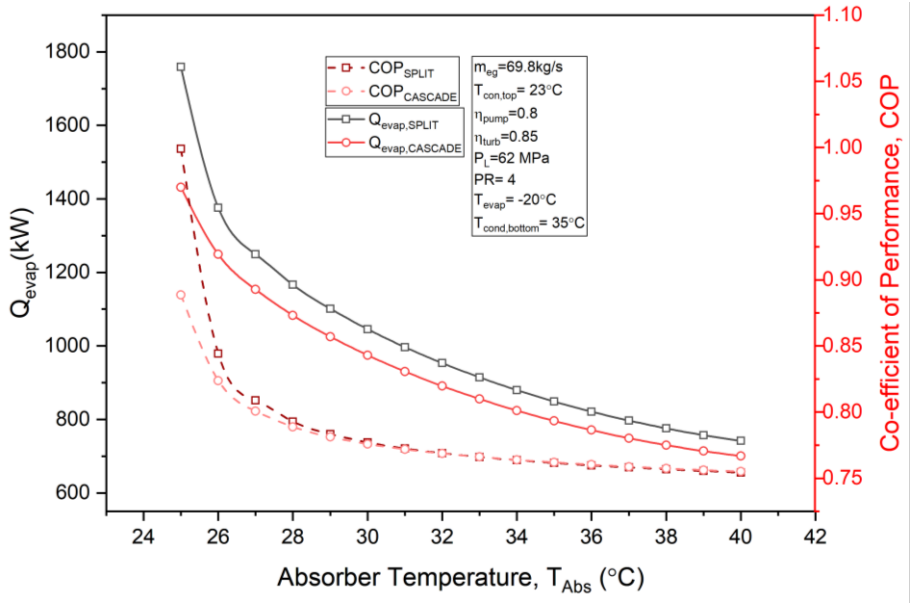

Figure 15: Effect of Absorber Temperature on cooling effect and COP.

The graph depicts the correlation between the absorber temperature (T_abs) and two significant performance indicators: the evaporator heat transfer rate (Q_evap) and the coefficient of performance (COP) for both the split and cascade cycles. The x-axis represents the temperature of the absorber (T_abs) in degrees Celsius. The y-axis on the left shows the rate at which heat is transferred in the evaporator (Q_evap) in kilowatts (kW), and the y-axis on the right indicates the coefficient of performance (COP). The graph displays four lines representing different variables: Q_evap for the split cycle, Q_evap for the cascade cycle, COP for the split cycle, and COP for the cascade cycle. The Q_evap lines are depicted as solid lines, with the split cycle represented by a black line with square markers, and the cascade cycle represented by a red line featuring circular markers. The COP lines are depicted as dashed, with the split cycle represented by a black line with square markers, and the cascade cycle represented by a red line featuring circular markers. With an increase in the absorber temperature, both the evaporator heat transfer rate (Q_evap) and the coefficient of performance (COP) drop for both cycles. Nevertheless, the split cycle regularly demonstrates superior Q_evap and COP values in comparison to the cascade cycle. This suggests that the split cycle demonstrates more efficiency in heat transfer and superior overall performance.The graph also displays various operational parameters that were maintained during the analysis. These parameters include the mass flow rate, which is 69.8 kg per

second, the top condenser temperature, which is 23 degrees Celsius, the pump efficiency, which is 0.8, the turbine efficiency, which is 0.85, the lower pressure, which is 62 MPa, the pressure ratio, which is 4, the evaporator temperature, which is -20 degrees Celsius, and the bottom condenser temperature, which is 35 degrees Celsius. Overall, the graph clearly shows that the split cycle surpasses the cascade cycle in terms of both evaporator heat transfer rate and coefficient of performance, regardless of the absorber temperature.

5.4 Effect of Evaporator Temperature (T_{evap})

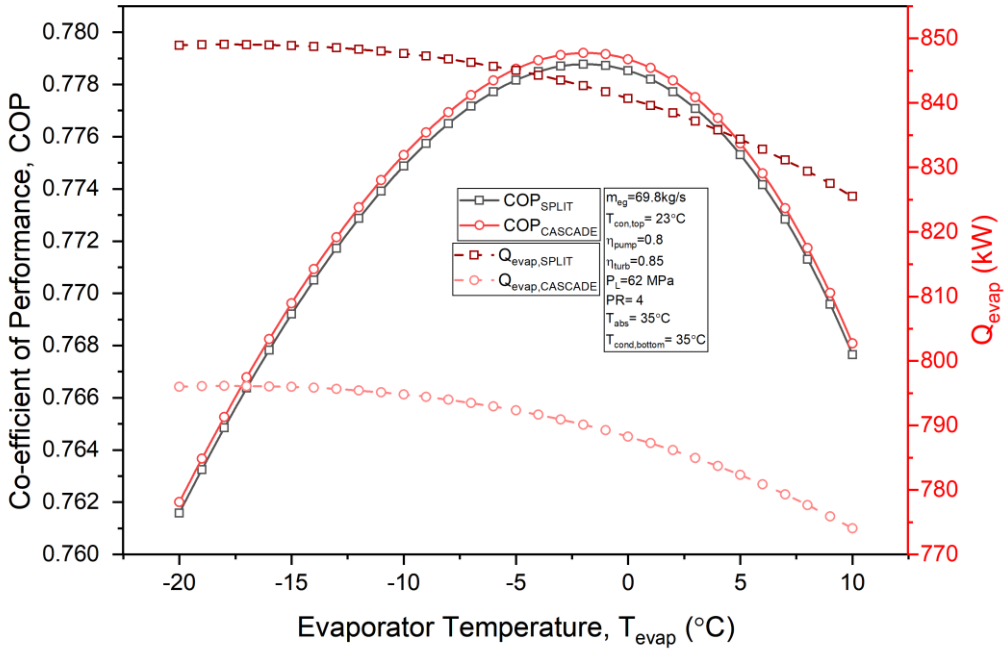

Figure 16: Effect of Evaporator Temperature on cooling effect and COP.

The graph illustrates the correlation between the evaporator temperature (Tevap) and two important performance indicators: the coefficient of performance (COP) and the evaporator heat transfer rate (Qevap) for both the split and cascade cycles. The x-axis represents the temperature of the evaporator in degrees Celsius. The y-axis on the left displays the coefficient of performance, while the y-axis on the right indicates the rate at which heat is transferred in the evaporator, measured in kilowatts (kW). The graph displays four lines representing the Coefficient of Performance (COP) for both the split cycle and cascade cycle, as well as the Evaporator Heat Transfer (Qevap) for both cycles. The COP lines are continuous, with the split cycle depicted as a black line with square markers and the cascade cycle as a red line with circular marks. The Qevap lines are depicted as dashes, with the split cycle indicated by a black line including square markers, and the cascade cycle represented by a red line with circular markers. As the temperature of the evaporator increases, the coefficient of performance (COP) for both the split and cascade cycles initially climbs, reaches a maximum point, and then starts to decrease. The split cycle consistently demonstrates superior coefficient of performance (COP) values in comparison to the cascade cycle, signifying a more efficient performance. The Qevap for both cycles exhibits

contrasting trends, with the split cycle exhibiting a larger rate of heat transfer across the whole temperature range in comparison to the cascade cycle. Nevertheless, when the temperature of the evaporator rises, the heat transfer rate at the evaporator (Qevap) rapidly diminishes for both cycles. The graph also displays other operational criteria that were upheld during the analysis: The mass flow rate is 69.8 kg/s, the top condenser temperature is 23°C, the pump efficiency is 0.8, the turbine efficiency is 0.85, the lower pressure is 62 MPa, the pressure ratio is 4, the absorber temperature is 35°C, and the bottom condenser temperature is 35°C. To summarize, the graph clearly shows that the split cycle surpasses the cascade cycle in terms of both the coefficient of performance and evaporator heat transfer rate across the whole range of evaporator temperatures. The higher performance of the split cycle can be due to its more efficient configuration and optimal working settings.

5.4 Effect of Condenser Temperature (T_{cond})(Bottom)

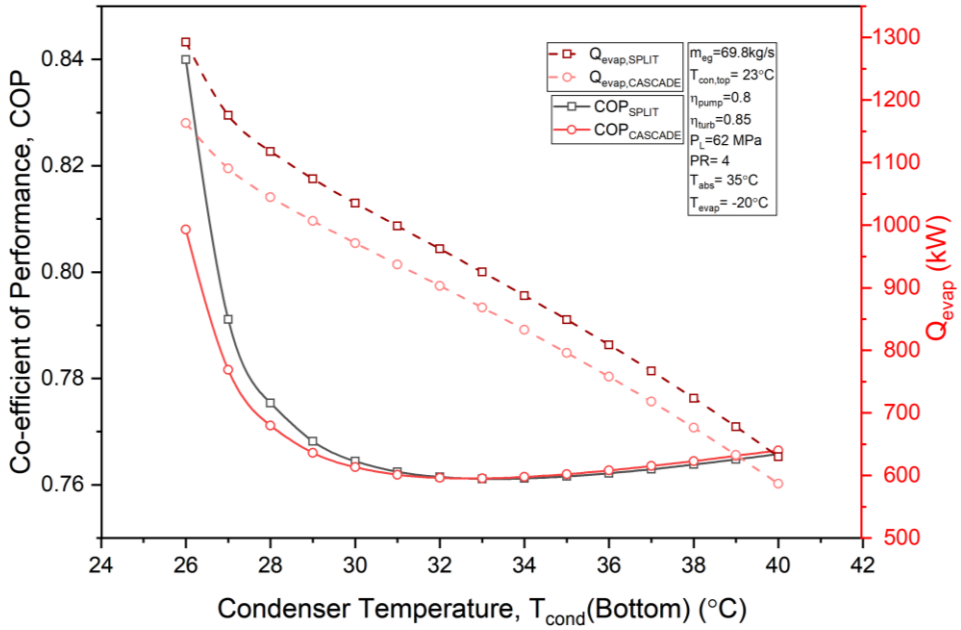

Figure 17: Effect of Condenser Temperature on COP.

The graph depicts the correlation between the bottom condenser temperature (Tcond) and two important performance indicators: the coefficient of performance (COP) and the evaporator heat transfer rate (Qevap) for both the split and cascade cycles. The x-axis depicts the temperature of the bottom condenser (Tcond) in degrees Celsius, while the left y-axis represents the coefficient of performance (COP), and the right y-axis indicates the rate of heat transfer in the evaporator (Qevap) in kilowatts (kW). The graph displays four lines representing the Coefficient of Performance (COP) for the split cycle, the COP for the cascade cycle, the evaporator heat transfer rate (Qevap) for the split cycle, and the Qevap for the cascade cycle. The COP lines are continuous, with the split cycle depicted by a black line with square indicators and the cascade cycle represented by a red line with circular indicators. The Qevap lines are depicted as dashes, with the split cycle illustrated by a black line including square markers, and the cascade cycle represented by a red line with circular

markers. As the temperature of the condenser at the bottom rises, both the coefficient of performance (COP) and the amount of heat absorbed during evaporation (Qevap) drop for both cycles. The split cycle routinely demonstrates superior Coefficient of Performance (COP) and evaporator heat transfer (Qevap) values in comparison to the cascade cycle. This suggests that the split cycle is superior in terms of both performance and heat transfer efficiency. The disparity in performance between the two cycles becomes more evident at lower condenser temperatures. The graph displays various operational parameters that were upheld during the analysis. These parameters include a mass flow rate of 69.8 kilograms per second, a top condenser temperature of 23 degrees Celsius, a pump efficiency of 0.8, a turbine efficiency of 0.85, a lower pressure of 62 MPa, a pressure ratio of 4, an absorber temperature of 35 degrees Celsius, and an evaporator temperature of -20 degrees Celsius. To summarize, the graph shows that the split cycle surpasses the cascade cycle in terms of both the coefficient of performance and evaporator heat transfer rate across the whole range of bottom condenser temperatures.

5.4 Effect of Condenser Temperature (T_{cond})(Top)

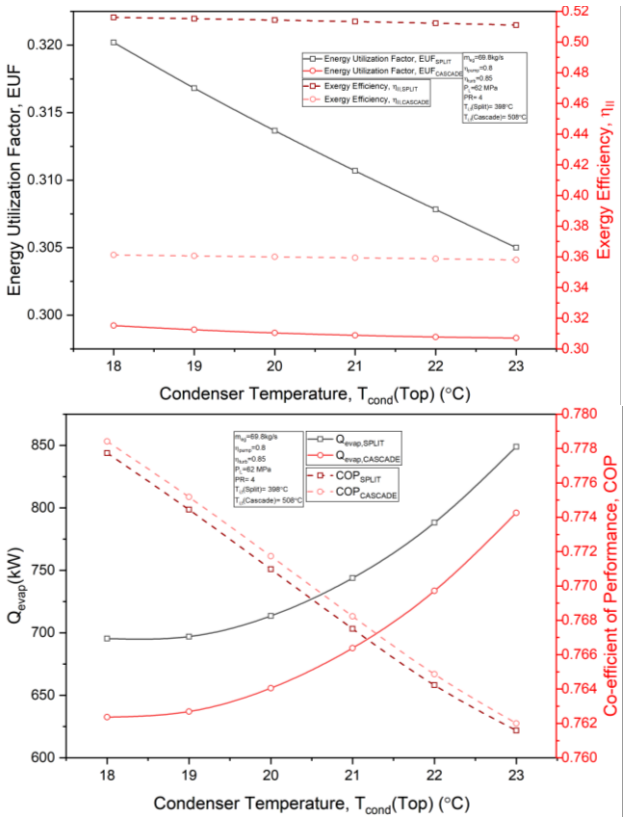

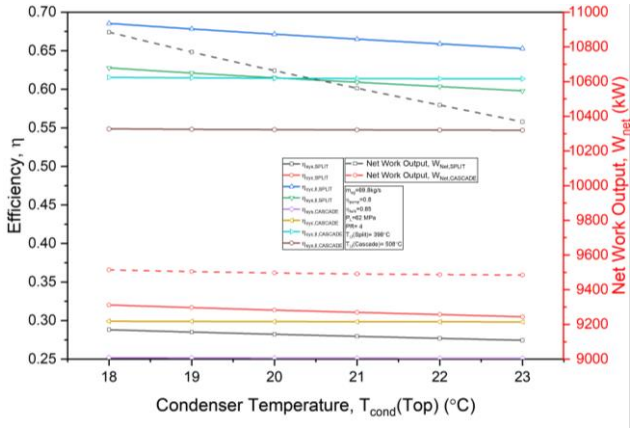

Figure 18: Effect of top condenser temperature on performance of the overall system.

The first graph depicts the correlation between the top condenser temperature (Tcond) and two performance indicators: the energy utilization factor (EUF) and the exergy efficiency, for both the split and cascade cycles. The x-axis reflects the temperature of the top condenser in degrees Celsius, while the left y-axis represents the energy utilization factor (EUF) and the right y-axis represents the exergy efficiency. The graph displays four lines representing the EUF (Energy Utilization Factor) for both the split cycle and cascade cycle, as well as the exergy efficiency for both cycles. The EUF lines are continuous, with the split cycle indicated by a black line with square markers and the cascade cycle indicated by a red line with circular markers. The exergy efficiency lines are represented by dashed lines. The split cycle is depicted by a black line with square markers, while the cascade cycle is represented by a red line with circular markers. As the temperature of the condenser increases, the energy utilization factor (EUF) drops for both cycles. The split cycle consistently demonstrates superior Energy Utilization Factor (EUF) values in comparison to the cascade cycle, suggesting its superior energy utilization capability. The exergy efficiency has a comparable downward trajectory, with the split cycle demonstrating superior exergy efficiency values in comparison to the cascade cycle. The analysis is conducted using the following operational parameters: a mass flow rate of 69.8 kilos per second, a pump efficiency of 0.8, a turbine efficiency of 0.85, a lower pressure of 62 MPa, a pressure ratio of 4, and particular temperatures for the split and cascade cycles. The second graph illustrates the correlation between the top condenser temperature (Tcond) and two important performance indicators: the evaporator heat transfer rate (Qevap) and the coefficient of performance (COP) for both the split and cascade cycles. The x-axis depicts the temperature of the top condenser in degrees Celsius. The y-axis on the left reflects the rate at which heat is transferred in the evaporator (Qevap) in kilowatts, and the y-axis on the right indicates the coefficient of performance (COP). The graph displays four lines representing the Coefficient of Performance (COP) for both the split cycle and cascade cycle, as well as the heat absorbed (Qevap) for both cycles. The COP lines are depicted as solid lines, with the split cycle represented by a black line featuring square markers, and the cascade cycle represented by a red line featuring circular markers. The Qevap lines are depicted as dashes, with the split cycle indicated by a black line including square markers, and the cascade cycle represented by a red line with circular markers. As the condenser temperature rises, the coefficient of performance (COP) declines for both cycles, with the split cycle consistently exhibiting

higher COP values. The Qevap, which represents the evaporation heat transfer rate, increases for both cycles. However, the split cycle exhibits higher heat transfer rates compared to the other cycle. This suggests that the split cycle demonstrates superior efficiency in terms of performance and heat transfer. The operational parameters remain unchanged from those depicted in the initial graph. The third graph illustrates the correlation between the top condenser temperature (Tcond) and two performance indicators: efficiency and net work production, for both the split and cascade cycles. The x-axis reflects the temperature of the top condenser in degrees Celsius, while the left y-axis shows the efficiency and the right y-axis indicates the net work production in kilowatts. The graph displays multiple lines that depict the efficiency of the first law and second law for both the system and cycle, as well as the net work production for both cycles. The efficiency lines are continuous, with distinct colors indicating the varied efficiencies for the split and cascade cycles. The dashed lines on the net work output graph depict the split cycle, indicated by a black line with square markers, and the cascade cycle, indicated by a red line with circular markers. As the condenser temperature rises, the efficiencies of both cycles typically decline, although the split cycle tends to maintain greater efficiency levels. The net work output declines for both cycles, with the split cycle exhibiting larger net work output values in comparison to the cascade cycle. The operational parameters align with those depicted in the previous graphs. To summarize, the three graphs show that the split cycle is superior to the cascade cycle in terms of energy usage, exergy efficiency, heat transfer rate, coefficient of performance, and net work production at various top condenser temperatures. The exceptional performance can be attributed to the ideal operating conditions and effective setup of the split cycle.

5.5 Effect of $T_{t,it}$ and P_L (Cascade)

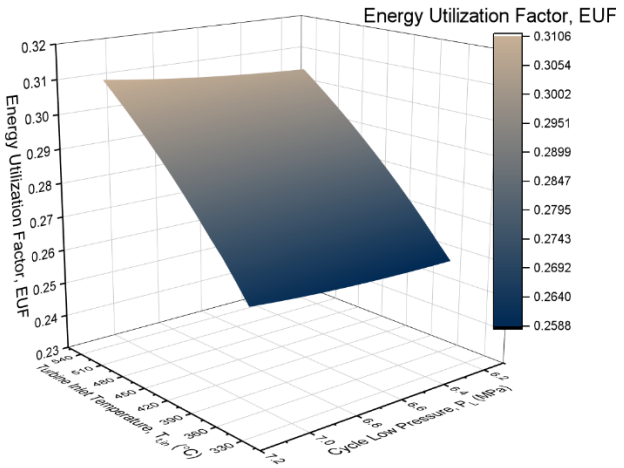

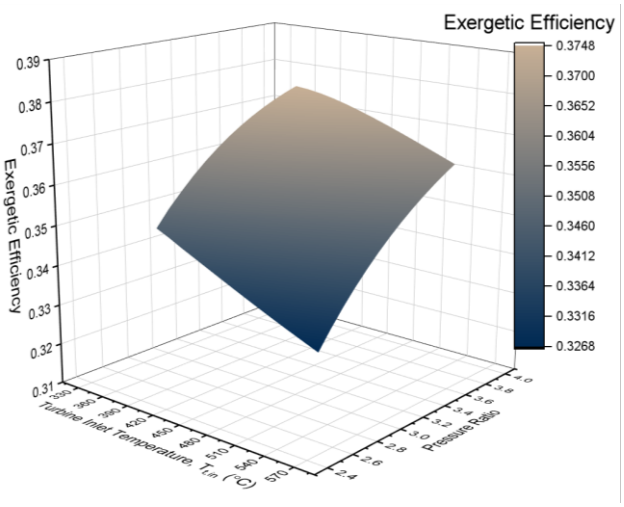

Figure 19: Three dimensional parametric analysis of turbine inlet temperature and cycle lower pressure.

The initial graph illustrates a three-dimensional surface plot that depicts the correlation between the turbine inlet temperature (Tin), cycle low pressure (P), and the energy utilization factor (EUF). The x-axis depicts the turbine inlet temperature in degrees Celsius, spanning from around 310 to 520 degrees. The y-axis depicts the minimum pressure throughout a cycle, measured in MPa, with a range from 0.1 to 2.2 MPa. The z-axis indicates the energy consumption factor, which varies between around 0.23 and 0.32. The surface plot illustrates the relationship between the energy utilization factor and variations in both the turbine input temperature and cycle low pressure. As the temperature at which the turbine is entered increases, the EUF typically increases. On the other hand, when the low pressure in the cycle lowers, the EUF likewise increases. The EUF values reach their maximum levels when the turbine inlet temperatures are elevated and the cycle low pressures are reduced. The color gradient on the surface plot, ranging from blue to tan, signifies the range of EUF values, with blue denoting lower levels and tan denoting higher ones. The second graph displays a three-dimensional surface plot illustrating the correlation between the turbine inlet temperature (Tin), pressure ratio, and the exergetic efficiency. The x-axis depicts the turbine inlet temperature in degrees Celsius, spanning from around 390 to 570 degrees. The y-axis depicts the pressure ratio, which spans from 2.4 to 4.0. The z-axis indicates the exergetic efficiency, which varies between approximately 0.31 and 0.39. The surface map illustrates the relationship between exergetic efficiency and variations in turbine inlet temperature and pressure ratio. As the temperature at which the turbine receives gas increases, the efficiency of the system in converting energy into useful work also improves. Similarly, as the ratio of pressure increases, the exergetic efficiency demonstrates a rising tendency. Exergetic efficiency ratings reach their peak at elevated turbine inlet temperatures and increased pressure ratios. The surface plot exhibits a color gradient that spans from blue to tan, indicating the range of exergetic efficiency values. Blue corresponds to lower values, while tan corresponds to higher values. Both graphs offer a detailed depiction of how the turbine inlet temperature and other factors, such as cycle low pressure and pressure ratio, impact the energy utilization factor and exergetic efficiency. These insights are essential for maximizing the performance and efficiency of thermodynamic cycles.

5.6 Effect of $T_{t,it}$ and P_L (Split)

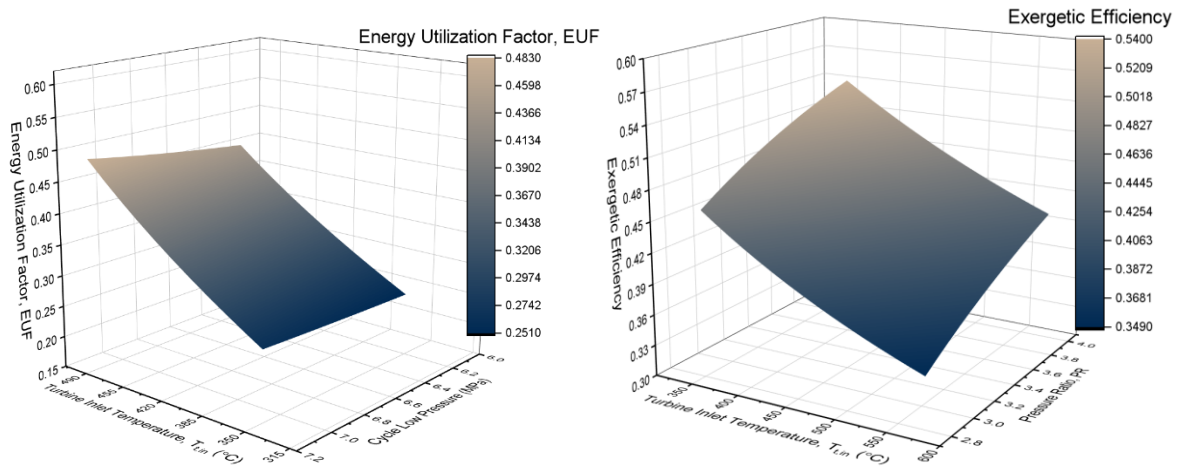

Figure 20: Three dimensional parametric analysis for split cascaded system.

The initial graph illustrates a three-dimensional surface plot depicting the correlation among the turbine input temperature, cycle low pressure, and the energy utilization factor. The x-axis depicts the turbine inlet temperature in degrees Celsius, spanning from around 315 to 450 degrees. The y-axis depicts the minimum pressure throughout a cycle, measured in megapascals (MPa), and ranges from 0.1 to 1.0 MPa. The z-axis depicts the energy utilization factor, which varies between approximately 0.25 and 0.48. The surface plot illustrates the relationship between the energy utilization factor and variations in both the turbine input temperature and cycle low pressure. As the temperature at which the turbine is fed with air increases, the efficiency of energy utilization typically increases. On the other hand, when the low pressure in the cycle drops, the energy utilization factor also increases. The maximum energy usage factor values are seen when the turbine inlet temperatures are greater and the cycle low pressures are lower. The surface plot exhibits a color gradient that spans from blue to tan, indicating the range of energy consumption factor values. Blue corresponds to lower values, while tan corresponds to higher ones. The second graph displays a three-dimensional surface plot illustrating the correlation among the turbine inlet temperature, pressure ratio, and exergetic efficiency. The x-axis depicts the turbine inlet temperature in degrees Celsius, spanning from around 490 to 600 degrees. The vertical axis corresponds to the pressure ratio, which spans from 2.0 to 4.0. The z-axis indicates the exergetic efficiency, which spans from around 0.35 to 0.54. The surface plot illustrates the relationship between changes in the turbine inlet temperature and pressure ratio and the corresponding variations in exergetic efficiency. As the temperature at which the turbine receives air increases, the efficiency of the energy conversion process also increases. Moreover, as the pressure ratio rises, the exergetic efficiency exhibits a corresponding upward trend. Exergetic efficiency ratings reach their peak at elevated turbine inlet temperatures and increased pressure ratios. The surface plot displays a color gradient that spans from blue to tan, indicating the range of exergetic efficiency values. Blue corresponds to lower values, while tan corresponds to higher ones. To summarize, these figures offer a thorough perspective on how the turbine inlet temperature

and other parameters, such as cycle low pressure and pressure ratio, affect the energy utilization factor and exergetic efficiency. These observations are essential for maximizing the effectiveness and productivity of thermodynamic cycles.

5.7 Exergy Analysis of the preferred System

The exergy diagram visually depicts the flow of energy and the degradation of exergy in the split system. The graphic starts with an exergy input of 17465.2 kilowatts. The input is divided into different system components, each of which either contributes to the overall exergy production or undergoes exergy destruction. Located on the left side of the diagram, we observe the exergy input and its subsequent allocation. Approximately 37.63 percent of the exergy input, which amounts to 6572.05 kilowatts, is lost as a result of exergy degradation in the power cycle. In addition, there is a loss of 123 kilowatts (0.7 percent) caused by the dissipation of exergy in the refrigeration cycle. The residual exergy is employed by various components within the system. The components consist of the following power outputs: compressor (651.46 kilowatts), pump (511.15 kilowatts), turbine (1205.38 kilowatts), recuperator (484.29 kilowatts), high-temperature heater (2162.20 kilowatts), and low-temperature heater (1567.21 kilowatts). The absorber, compressors 1 and 2, condenser, evaporator, throttle valve, flash tank, and generator also require an exergy input. The absorber requires 275.56 kilowatts, compressor 1 requires 751.37 kilowatts, compressor 2 requires 515.15 kilowatts, condenser requires 332.10 kilowatts, evaporator requires 92.80 kilowatts, throttle valve requires 7.37 kilowatts, flash tank requires 95.17 kilowatts, and generator requires 44.13 kilowatts. In addition, the exergy distribution within the system is attributed to individual components such as the mixing chamber (19.97 kilowatts), RHX (7.37 kilowatts), SHX (8.08 kilowatts), TV III (2.33 kilowatts), and other components. The system's exergy production amounts to 10770.15 kilowatts, accounting for 61.66 percent of the initial exergy input. This output represents the effectiveness of the system in turning the input exergy into productive work, taking into account the losses caused by exergy destruction in different components of the system. The graphic aptly depicts the exergy flow and losses, facilitating a thorough comprehension of the system's performance.

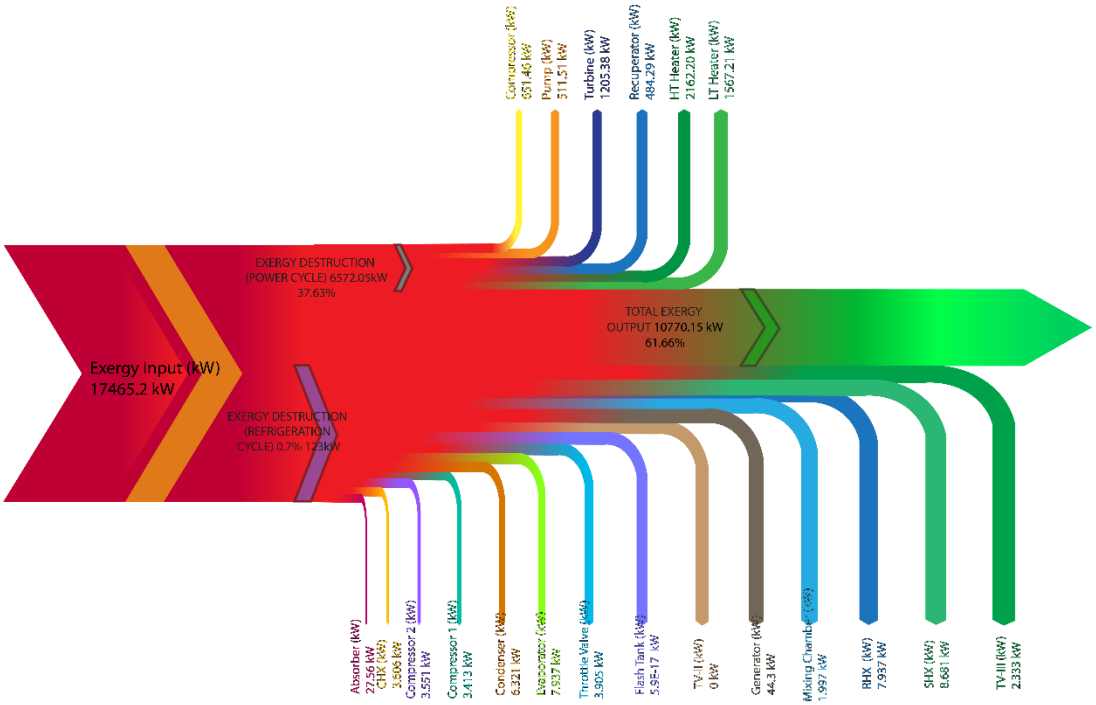

Figure 21: Visual representation of exergetic analysis.

Chapter 6 Conclusion

Overall, this extensive analysis compares a new Cascade Transcritical CO2 cycle and a new Split Transcritical CO2 cycle, both combined with an Advanced Absorption Refrigeration system. It offers detailed insights into their performance in terms of energy and exergy. The analysis emphasizes the greater efficiency of the split cycle under different operational situations, making it a more feasible choice for combined power and cooling applications.

- The split cycle consistently demonstrates higher coefficients of performance (COP) compared to the cascade cycle. This indicates that the split cycle is more efficient in converting energy inputs into useful work and cooling output.
- The energy utilization factor (EUF) and exergy efficiency are significantly higher in the split cycle, indicating a more effective use of energy inputs and lower energy losses.
- Detailed analysis of operational parameters such as turbine inlet temperature, cycle low pressure, and pressure ratio reveals that the split cycle maintains superior performance across a range of conditions. The turbine inlet temperature, in particular, has a notable impact on the efficiency metrics, with higher temperatures generally improving performance.
- Exergy analysis highlights the importance of minimizing exergy destruction to improve overall system efficiency. The split cycle shows a remarkable ability to reduce exergy losses, resulting in a higher total exergy output. This is crucial for applications that require both high efficiency and sustainability.
- Exergy destruction in the power cycle and refrigeration cycle is lower in the split cycle, underscoring its design advantages in preserving the quality of energy throughout the system.
- The integration of an Advanced Absorption Refrigeration system enhances the cooling performance of both cycles. However, the split cycle benefits more from this integration, further boosting its efficiency and effectiveness.
- This integrated approach not only improves thermal performance but also offers a sustainable solution by reducing the overall energy consumption and environmental impact.
- The findings suggest that the split cycle's design, which minimizes exergy destruction and maximizes energy utilization, can be optimized further to achieve even greater efficiencies. Fine-tuning parameters such as pressure ratios and inlet temperatures can lead to significant performance improvements.
- These insights are critical for the development of next-generation energy systems that are both high-performing and environmentally friendly.
- By reducing exergy destruction and improving energy efficiency, the split cycle contributes to lower carbon emissions and a smaller environmental footprint. This makes it an attractive option for industries looking to adopt sustainable practices.
- The improved efficiency also translates to cost savings in terms of energy consumption, making the split cycle a cost-effective solution for long-term operation.
- The superior performance of the split cycle makes it suitable for a wide range of applications, including industrial cooling, power generation, and combined heat and power (CHP) systems.
- Future research can explore further optimization strategies, such as advanced control systems and novel materials, to enhance the performance of the split cycle even more.
- Investigating the integration of renewable energy sources with the split cycle could also offer additional environmental benefits and further reduce reliance on fossil fuels.

Overall, this study underscores the significant advantages of the split cycle over the cascade cycle in terms of energy and exergy efficiency. The split cycle's optimal configuration, ability to minimize exergy destruction, and effective use of energy inputs make it a promising solution for future energy systems. These insights provide a strong foundation for ongoing research and development, aimed at creating more efficient, sustainable, and cost-effective energy solutions. The split cycle's performance highlights its potential to lead the way in the transition towards more sustainable industrial practices and energy systems.

6.1 Limitations and Future Recommendations

While the presented systems have various possibilities and originality, it is crucial to acknowledge that there are still limitations in this research. Additional enhancements can be implemented by addressing the aforementioned constraints.

Limitations

- The thermodynamic modelling assumption involves implementing certain necessary assumptions to simplify the numerical analysis and develop the system. These assumptions may not align with the actual circumstances in the real world. There are possible opportunities for future advancement of this project that involve taking into account more specific elements like as heat losses, pressure drop, and component efficiency.
- The implementation scope of the created model primarily focuses on a limited number of operational characteristics. However, it is important to note that there are several other factors to consider in real-world scenarios, such as long-term viability, environmental impact, and economic expenses.
- Experimental study is necessary to fully comprehend the capabilities of these innovative systems in real-world applications. This research will involve validating prototypes through evaluation.

Recommendations

In order to enhance the potential for progress in this study, below are few recommendations that will aid in a deeper understanding and enrichment of this particular research domain.

- Advanced exergy analysis can be used to determine the comprehensive contribution of a component to exergy destruction. This analysis helps to identify the extent to which exergy destruction can be minimised. In addition, exergonomic analysis can be conducted to incorporate the economic dimension.
- Optimisation: Utilising multi-objective optimisation might be a viable approach to maximise the output parameters while taking into account their correlation with each other. Optimisation is the process of identifying the optimal values for a given parameter within a specific range in order to achieve the most efficient outcome. Further research can explore the possibilities of this endeavour.

- Empirical Evaluation: The process of conducting real-world testing and validation is essential to ensure the design of systems that are appropriate for actual application. Empirical experiments are crucial for advancing research in this industry.
- The proposed novel systems have the potential to incorporate renewable energy sources as the main heat input. This allows for a realistic opportunity to integrate cascaded refrigeration systems with sustainable energy sources. This positive collaboration has the potential to greatly enhance this sector by making cooling methods more feasible and efficient.

References

[1] Y. M. Kim, J. L. Sohn, and E. S. Yoon, “Supercritical CO2 Rankine cycles for waste heat recovery from gas turbine,” *Energy*, vol. 118, pp. 893–905, Jan. 2017, doi: 10.1016/J.ENERGY.2016.10.106.

[2] D. Alfani, M. Binotti, E. Macchi, P. Silva, and M. Astolfi, “sCO2 power plants for waste heat recovery: design optimization and part-load operation strategies,” *Appl Therm Eng*, vol. 195, p. 117013, Aug. 2021, doi: 10.1016/J.APPLTHERMALENG.2021.117013.

[3] I. Dincer and M. A. Rosen, “Chemical exergy,” *Exergy*, pp. 37–60, 2021, doi: 10.1016/B978-0-12-824372-5.00003-8.

[4] I. Dincer and M. A. Rosen, “Thermodynamic fundamentals,” *Exergy*, pp. 1–22, 2021, doi: 10.1016/B978-0-12-824372-5.00001-4.

[5] Y. M. Kim, J. L. Sohn, S. Yoon, and S. Korea, “Supercritical CO 2 Rankine cycles for waste heat recovery from gas turbine”, doi: 10.1016/j.energy.2016.10.106.

[6] M. W. Faruque, Y. Khan, M. H. Nabil, and M. M. Ehsan, “Parametric analysis and optimization of a novel cascade compression-absorption refrigeration system integrated with a flash tank and a reheater,” *Results in Engineering*, vol. 17, p. 101008, Mar. 2023, doi: 10.1016/J.RINENG.2023.101008.

[7] I. Dincer and M. A. Rosen, “Exergy and energy analyses,” *Exergy*, pp. 23–35, 2021, doi: 10.1016/B978-0-12-824372-5.00002-6.

[8] Z. Bai, G. Zhang, Y. Li, G. Xu, and Y. Yang, “A supercritical CO2 Brayton cycle with a bleeding anabranch used in coal-fired power plants,” *Energy*, vol. 142, pp. 731–738, Jan. 2018, doi: 10.1016/J.ENERGY.2017.09.121.

[9] M. E. Tat, “Cetane number effect on the energetic and exergetic efficiency of a diesel engine fuelled with biodiesel,” *Fuel Processing Technology*, vol. 92, no. 7, pp. 1311–1321, Jul. 2011, doi: 10.1016/J.FUPROC.2011.02.006.

[10] M. Saghafifar, A. Omar, K. Mohammadi, A. Alashkar, and M. Gadalla, “A review of unconventional bottoming cycles for waste heat recovery: Part I – Analysis, design, and optimization,” *Energy Convers Manag*, vol. 198, p. 110905, Oct. 2019, doi: 10.1016/J.ENCONMAN.2018.10.047.

[11] F. Zhang *et al.*, “Proposal and performance assessment of a combined system based on a supercritical carbon dioxide power cycle integrated with a double-effect absorption power cycle,” *Energy Convers Manag*, vol. 233, p. 113923, Apr. 2021, doi: 10.1016/J.ENCONMAN.2021.113923.

[12] C. P. Jawahar and R. Saravanan, “Experimental studies on air-cooled NH3–H2O based modified gax absorption cooling system,” *International Journal of Refrigeration*, vol. 34, no. 3, pp. 658–666, May 2011, doi: 10.1016/J.IJREFRIG.2010.11.005.

[13] M. S. Kim, Y. Ahn, B. Kim, and J. I. Lee, “Study on the supercritical CO2 power cycles for landfill gas firing gas turbine bottoming cycle,” *Energy*, vol. 111, pp. 893–909, Sep. 2016, doi: 10.1016/J.ENERGY.2016.06.014.

[14] L. Wang, L. ming Pan, J. Wang, D. Chen, Y. Huang, and L. Hu, “Investigation on the temperature sensitivity of the S-CO2 Brayton cycle efficiency,” *Energy*, vol. 178, pp. 739–750, Jul. 2019, doi: 10.1016/J.ENERGY.2019.04.100.

[15] Y. M. Kim, J. L. Sohn, and E. S. Yoon, “Supercritical CO2 Rankine cycles for waste heat recovery from gas turbine,” *Energy*, vol. 118, pp. 893–905, Jan. 2017, doi: 10.1016/J.ENERGY.2016.10.106.

[16] M. Atif and F. A. Al-Sulaiman, “Development of a mathematical model for optimizing a heliostat field layout using differential evolution method,” *Int J Energy Res*, vol. 39, no. 9, pp. 1241–1255, Jul. 2015, doi: 10.1002/ER.3325.

[17] M. Atif and F. A. Al-Sulaiman, “Optimization of heliostat field layout in solar central receiver systems on annual basis using differential evolution algorithm,” *Energy Convers Manag*, vol. 95, pp.

1–9, May 2015, doi: 10.1016/J.ENCONMAN.2015.01.089.

[18] O. Kizilkan and H. Yamaguchi, “Feasibility research on the novel experimental solar-assisted CO2 based Rankine cycle integrated with absorption refrigeration,” *Energy Convers Manag*, vol. 205, Feb. 2020, doi: 10.1016/J.ENCONMAN.2019.112390.

[19] O. Kizilkan, S. Khanmohammadi, and H. Yamaguchi, “Two-objective optimization of a transcritical carbon dioxide based Rankine cycle integrated with evacuated tube solar collector for power and heat generation,” *Appl Therm Eng*, vol. 182, Jan. 2021, doi: 10.1016/J.APPLTHERMALENG.2020.116079.

[20] M. A. Reyes-Belmonte, A. Sebastián, M. Romero, and J. González-Aguilar, “Optimization of a recompression supercritical carbon dioxide cycle for an innovative central receiver solar power plant,” *Energy*, vol. 112, pp. 17–27, Oct. 2016, doi: 10.1016/J.ENERGY.2016.06.013.

[21] Z. Bai, G. Zhang, Y. Li, G. Xu, and Y. Yang, “A supercritical CO2 Brayton cycle with a bleeding anabranch used in coal-fired power plants,” *Energy*, vol. 142, pp. 731–738, Jan. 2018, doi: 10.1016/J.ENERGY.2017.09.121.

[22] F. Crespi, G. Gavagnin, D. Sánchez, and G. S. Martínez, “Supercritical carbon dioxide cycles for power generation: A review,” *Appl Energy*, vol. 195, pp. 152–183, 2017, doi: 10.1016/J.APENERGY.2017.02.048.

[23] J. Zhang, “A SYSTEMATIC COMPARISON OF SUPERCRITICAL CO2 BRAYTON CYCLE LAYOUTS FOR CONCENTRATED SOLAR POWER WITH A FOCUS ON THERMAL ENERGY STORAGE UTILIZATION,” 2019.

[24] Y. Li, J. Yu, H. Qin, Z. Sheng, and Q. Wang, “An experimental investigation on a modified cascade refrigeration system with an ejector,” *International journal of refrigeration*, vol. 96, pp. 63–69, Dec. 2018, doi: 10.1016/J.IJREFRIG.2018.09.015.

[25] H. Wang, Y. Song, and F. Cao, “Experimental investigation on the pull-down performance of a -80°C ultra-low temperature freezer,” *International Journal of Refrigeration-revue Internationale Du Froid*, vol. 119, pp. 1–10, Nov. 2020, doi: 10.1016/J.IJREFRIG.2020.04.030.

[26] D. Liang, M. Ibrahim, T. Saeed, A. M. El-Refaey, Z. Li, and M. A. Fagiry, “Simulation of a Trombe wall with a number of semicircular fins placed on the absorber plate for heating a room in the presence of nano-PCM,” *Journal of Building Engineering*, vol. 50, Jun. 2022, doi: 10.1016/J.JOBE.2022.104173.

[27] F. A. Almehmadi, K. P. Hallinan, R. B. Mulford, and S. A. Alqaed, “Technology to Address Food Deserts: Low Energy Corner Store Groceries with Integrated Agriculture Greenhouse,” *Sustainability*, vol. 12, no. 18, Sep. 2020, doi: 10.3390/SU12187565.

[28] S. Alqaed, J. Mustafa, M. Sharifpur, and G. Cheraghian, “Using nanoparticles in solar collector to enhance solar-assisted hot process stream usefulness,” *Sustainable Energy Technologies and Assessments*, vol. 52, Aug. 2022, doi: 10.1016/J.SETA.2022.101992.

[29] N. Johnson, J. Baltrusaitis, and W. L. Luyben, “Design and control of a cryogenic multi-stage compression refrigeration process,” *Chemical Engineering Research & Design*, vol. 121, pp. 360–367, 2017, doi: 10.1016/J.CHERD.2017.03.018.

[30] I. Kayes, R. E. Ratul, A. Abid, F. B. Majmader, Y. Khan, and M. M. Ehsan, “Multi-objective optimization and 4E (energy, exergy, economy, environmental impact) analysis of a triple cascade refrigeration system,” *Heliyon*, vol. 10, no. 11, Jun. 2024, doi: 10.1016/J.HELIYON.2024.E31655.

[31] Z. Liu, K. Yuan, Y. Ling, H. Tan, and S. Yang, “Experimental study on a -86 °C cascade refrigeration unit with environmental-friendly refrigerants R290-R170,” *Environ Sci Pollut Res Int*, vol. 30, no. 43, pp. 97339–97352, Sep. 2023, doi: 10.1007/S11356-023-29240-Y.

[32] S. Alqaed, “Effect of annual solar radiation on simple façade, double-skin facade and double-skin facade filled with phase change materials for saving energy,” *Sustainable Energy Technologies and Assessments*, vol. 51, Jun. 2022, doi: 10.1016/J.SETA.2021.101928.

[33] C. Vereda, R. Ventas, A. Lecuona, and R. López, “Single-effect absorption refrigeration cycle boosted with an ejector-adiabatic absorber using a single solution pump,” *International Journal of Refrigeration*, vol. 38, no. 1, pp. 22–29, Feb. 2014, doi: 10.1016/J.IJREFRIG.2013.10.010.

[34] A. M. Abed, M. A. Alghoul, R. Sirawn, A. N. Al-Shamani, and K. Sopian, “Performance enhancement of ejector-absorption cooling cycle by re-arrangement of solution streamlines and adding RHE,” *Appl Therm Eng*, vol. 77, pp. 65–75, Feb. 2015, doi: 10.1016/J.APPLTHERMALENG.2014.12.003.

[35] R. Gomri, “Second law comparison of single effect and double effect vapour absorption refrigeration systems,” *Energy Convers Manag*, vol. 50, no. 5, pp. 1279–1287, May 2009, doi: 10.1016/J.ENCONMAN.2009.01.019.

[36] M. U. Arshad, M. U. Ghani, A. Ullah, A. Güngör, and M. Zaman, “Thermodynamic analysis and optimization of double effect absorption refrigeration system using genetic algorithm,” *Energy Convers Manag*, vol. 192, pp. 292–307, Jul. 2019, doi: 10.1016/J.ENCONMAN.2019.03.083.

[37] R. Maryami and A. A. Dehghan, “An exergy based comparative study between LiBr/water absorption refrigeration systems from half effect to triple effect,” *Appl Therm Eng*, vol. 124, pp. 103–123, Sep. 2017, doi: 10.1016/J.APPLTHERMALENG.2017.05.174.

[38] A. Razmi, M. Soltani, F. M. Kashkooli, and L. Garousi Farshi, “Energy and exergy analysis of an environmentally-friendly hybrid absorption/recompression refrigeration system,” *Energy Convers Manag*, vol. 164, pp. 59–69, May 2018, doi: 10.1016/J.ENCONMAN.2018.02.084.

[39] A. R. Razmi, A. Arabkoohsar, and H. Nami, “Thermoeconomic analysis and multi-objective optimization of a novel hybrid absorption/recompression refrigeration system,” *Energy*, vol. 210, p. 118559, Nov. 2020, doi: 10.1016/J.ENERGY.2020.118559.